

# The Luminous Starburst Ring in NGC 7771: Sequential Star Formation?<sup>1</sup>

Denise A. Smith

Space Telescope Science Institute  
3700 San Martin Drive  
Baltimore, MD 21218  
Electronic Mail: dsmith@stsci.edu

Terry Herter and Martha P. Haynes  
Center for Radiophysics and Space Research  
Space Sciences Building  
Cornell University, Ithaca, NY 14853

Susan G. Neff  
NASA Goddard Space Flight Center  
Code 681  
Greenbelt, MD 20771

## ABSTRACT

Only two of the twenty highly luminous starburst galaxies analyzed by Smith et al. exhibit circumnuclear rings of star formation. These galaxies provide a link between  $\sim 10^{11} L_{\odot}$  luminosity class systems and classical, less-luminous ringed systems. In this paper, we report the discovery of a near-infrared counterpart to the 1.6 kpc diameter nuclear ring of radio emission in NGC 7771 (UGC 12815). The ring contains  $\approx 10$  radio bright clumps and  $\approx 10$  near-infrared bright clumps. A displacement between the peaks of the radio and the near-infrared emission indicates the presence of multiple generations of star formation. The estimated thermal emission from each radio source is equivalent to that of  $\sim 35000$  O6 stars. Each near-infrared bright knot contains  $\sim 5000$  red supergiants, on average. In the case that the radio-bright knots are 4 Myr old and the near-infrared bright knots are  $\approx 10$  Myr old, each knot is characterized by a stellar mass of  $10^7 M_{\odot}$ , and the implied time-averaged star formation rate is  $\sim 40 M_{\odot} \text{ yr}^{-1}$ . Several similarities are found between the properties of this system and other ringed and non-ringed starbursts. Morphological differences between NGC 7771 and the starburst + Seyfert 1 galaxy NGC 7469 (UGC 12332) suggest that NGC 7771 may not be old enough to fuel an AGN, or may not be capable of fueling an AGN. Alternatively, the differences may be unrelated to the presence or absence of an AGN and may simply reflect the possibility that star formation in rings is episodic.

---

<sup>1</sup>Observations at the Palomar Observatory were made as part of a continuing collaborative agreement between the California Institute of Technology and Cornell University.

*Subject headings:* galaxies: individual: (NGC 7771) — galaxies: starburst — galaxies: interactions — infrared: galaxies — galaxies: stellar content — galaxies: nuclei

## 1. Introduction

In order to better understand the nature of star formation occurring in nearby starburst galaxies and to provide a foundation for studies of higher redshift systems, we have been analyzing the properties of the 20 starburst galaxies with the highest 5 GHz luminosities from Condon, Frayer, & Broderick (1991). These galaxies form a sample of relatively nearby, northern hemisphere starbursts which is independent of the dust content and the morphology of the host galaxy. An example of our data and analysis technique is given in Smith et al. (1995), hereafter Paper 1. The complete sample and dataset are described in Smith et al. (1996), hereafter Paper 2, and are analyzed in Smith, Herter, & Haynes (1998), hereafter Paper 3. Since our near-infrared imaging data indicate the presence of strong central peaks of star formation, a program has been undertaken to obtain high-resolution near-infrared images of the cores of these galaxies, with the goal of improving our understanding of the origin and evolution of the activity in these systems.

In this paper, we report the discovery of a luminous near-infrared counterpart to the ring of 6 cm radio emission in the galaxy NGC 7771 (UGC 12815) (Neff & Hutchings 1992). Of the 20 very luminous starburst galaxies studied in Paper 3, only two contain circumnuclear starburst rings: NGC 7771 and NGC 7469 (UGC 12332). The properties of NGC 7469 are discussed in detail by Genzel et al. (1995), and references therein. In contrast to NGC 7771, NGC 7469 also contains a Seyfert 1 nucleus. Examples of less luminous galaxies containing circumnuclear rings which are and are not accompanied by a central AGN are plentiful in the literature (e.g. Buta & Crocker 1993, Schinnerer et al. 1997, Devereux, Kenney, & Young 1992, Storchi-Bergmann, Wilson, & Baldwin 1996, Buta 1986b, Maoz et al. 1996). The galaxies NGC 7771 and NGC 7469 thus serve as links between highly luminous objects and well-studied, lower luminosity galaxies characterized by circumnuclear rings and provide testbeds for theories concerning the evolution of luminous starbursts, ringed systems, and AGN.

The barred Sa galaxy NGC 7771 ( $D = 56.7$  Mpc,  $H_0 = 75$  km s<sup>-1</sup> Mpc<sup>-1</sup>) belongs to Lyon Galaxy Group #483 (Garcia 1993). This group, whose central velocity is 4506 km s<sup>-1</sup>, is also called the NGC 7771 Group and is comprised of NGC 7769, NGC 7771, NGC 7786, NGC 7770, and UGC 12828. Nordgren et al. (1997) have recently confirmed that a small object located to the west of NGC 7771 (NGC 7771A) is also a dynamical member of the group. NGC 7770 and NGC 7771 are identified as a pair (KPG 592) by Karachentsev (1987). NGC 7771 itself is clearly disturbed, as evidenced by the rotation curve described by Keel (1993), the HI profile obtained by Hutchings (1989), the HI tail found by Nordgren et al. (1997), and the optical morphology discussed by Burns et al. (1987) and by Nordgren et al. (1997). The HI velocity field confirms that

NGC 7771 is interacting with NGC 7769 and NGC 7771A (Nordgren et al. 1997). The interactions between the group members appear to have deposited large quantities of gas in NGC 7771; this object has a molecular hydrogen mass of  $M(\text{H}_2) = 8.91 \times 10^9 M_\odot$  (Sanders et al. 1986). Heavy extinction is also present, as evidenced by the patchy emission and the dust lane observed in the  $I$  band image shown in Figure 1. This image was obtained by R. Giovanelli and M. Haynes (private communication) with the 0.9m telescope at Kitt Peak National Observatory<sup>1</sup> under non-photometric conditions and  $1.6''$  seeing. A large scale bar visible in optical and near-infrared images at  $PA \sim 70 - 75^\circ$  may be channeling gas into the nuclear regions of NGC 7771 (Osman 1986; Paper 2; Figure 1).

Previous studies indicate that NGC 7771 is experiencing an intense burst of star formation and that it does not contain an active galactic nucleus (AGN). The ratio of the radio and the optical fluxes is higher than average for a spiral galaxy, suggesting the presence of an emission source other than “normal” disk emission. The similarity of the radio/optical flux ratio and the radio/far-infrared flux ratio to those of starburst galaxies and the lack of a strong, compact radio source suggest that the emission from NGC 7771 is powered by intense star formation, as opposed to an AGN (Condon, Frayer, & Broderick 1991; Batuski, Hanisch, & Burns 1992). Finally, optical line ratios indicate the presence of star formation activity and show no evidence of an AGN (Veilleux et al. 1995). The starburst activity is presumably the result of the interactions between NGC 7771 and members of the NGC 7771 Group.

With a far-infrared luminosity of  $L_{fir} = 2 \times 10^{11} L_\odot$ , the starburst in NGC 7771 is considerably more active than that occurring in the “prototypical” starburst galaxy M 82 ( $L_{fir} = 3 \times 10^{10} L_\odot$ ). High resolution ( $0.4''$  FWHM) 6 cm observations using the VLA A array resolve this starburst activity into a nuclear source and a circumnuclear ring-like structure  $6''$  (1.6 kpc) in diameter (Neff & Hutchings 1992). The structure of the radio emission is shown in Figure 2, along with our adopted nomenclature for the radio-bright circumnuclear knots. Near-infrared  $0.9''$  FWHM images obtained by Eales et al. (1990) indicate the presence of extended  $2 \mu\text{m}$  emission in the vicinity of the circumnuclear ring of radio emission. Since near-infrared spectroscopy suggests that young red supergiants are present in the central regions of NGC 7771 (Paper 3), a comparison between the radio and the near-infrared emission provides a valuable opportunity to trace the evolution of the starburst. Below, we discuss the results of  $0.6''$  FWHM resolution near-infrared imaging and their implications concerning the origin and evolution of the starburst in NGC 7771.

---

<sup>1</sup>Kitt Peak National Observatory, National Optical Astronomy Observatories, is operated by AURA, Inc. under a cooperative agreement with the National Science Foundation.

## 2. Observations and Data Reduction

NGC 7771 was observed in the standard  $J$ ,  $H$ , and  $K$  bands with the Caltech Cassegrain Infrared Camera at the 5m Hale telescope on 25 October 1994. The camera utilizes a  $256 \times 256$  InSb array with a scale of  $0.125'' \text{ pixel}^{-1}$ , and follows the CIT photometric system. The nuclear starburst region is easily imaged within the resulting  $32''$  field of view. Observations consisted of a series of alternating source and sky exposures. The galaxy was observed at multiple positions on the array in order to minimize any possible instrumental effects. Sky frames were taken to the north, south, east, and west of NGC 7771 using a  $2'$  nod, which is sufficient to move beyond the optical extent of the galaxy. Exposure times ranged from 10 s at  $K$ , 40 s at  $H$ , to 150 s at  $J$ . The efficiency of the  $H$  and  $K$  band data acquisition was increased by coadding multiple frames at each position. We observed NGC 7771 for a total of 460 s at  $K$ , 360 s at  $H$ , and 600 s at  $J$ . Stable seeing conditions ( $0.6''$  FWHM in all three bands) were present throughout the observations.

Standard data reduction procedures were applied to the data. A full discussion of general data reduction techniques may be found in Paper 1 and in Paper 2 and will not be repeated here. In summary, the data were linearized, sky-subtracted, and then flat-fielded. Images were aligned according to the position of the centroid of the galaxy nucleus in each frame, and then mosaicked. Since thin cirrus was present during the data acquisition, the fluxes quoted in Paper 2 were used to calibrate the data. These fluxes are the most accurate of those found in the literature to date. The colors of a  $5''$  aperture,  $H - K = 0.53 \pm 0.10$  mag and  $J - H = 0.84 \pm 0.06$  mag, are in excellent agreement with those of Carico et al. (1988), who derive  $H - K = 0.53 \pm 0.12$  mag and  $J - H = 0.91 \pm 0.12$  mag. The comparison between the two datasets suggests that the formal uncertainty in the  $H - K$  color may be an overestimate. Fluxes and colors were derived for the current dataset with a synthetic circular aperture  $0.75''$  in diameter. This aperture size was selected as a compromise between a  $1.25''$  diameter aperture, which collects all of the flux from an isolated  $0.6''$  FWHM point source, and one which best isolates the observed features. Observations of isolated point sources indicate that a  $0.75''$  aperture integrates 50% of the total flux emitted by a  $0.6''$  FWHM point source. Uncertainties were derived and quantities were corrected for redshift as in Paper 2. The redshift corrections are small ( $\leq 0.02$  mJy). The uncertainties are dominated by that of the flux calibration. Color transformations were not necessary since both the calibration fluxes and the Cassegrain Infrared Camera utilize the CIT photometric system.

Color maps were formed from the flux-calibrated images by aligning a prominent feature observed in all three bands (feature Kg in Figure 3, see below). The nucleus cannot be used to align the images since its  $J$  band morphology differs significantly from its  $H$  and  $K$  band morphologies. In the  $J$  band, the distinctness of the nucleus is compromised by the presence of extended emission to the northeast. The centroid of the nucleus itself is therefore not well determined in the  $J$  band. We confirmed the image alignment by blinking the registered images and by comparing the resulting color maps to lower resolution data obtained with the Prime Focus Infrared Camera (PFIRcam) (Paper 2). Low-resolution color maps were re-derived from the PFIRcam data presented in Paper 2 by aligning the point source located in the eastern arm of

NGC 7771. The high-resolution data were smoothed and rebinned to match the PFIRcam spatial resolution and sampling. We find good agreement between the two sets of color maps.

### 3. Results

#### 3.1. Morphology

The  $K$  band image of the nuclear starburst region is displayed in greyscale in Figure 3 along with the nomenclature of the various knots. Contours representing the ring of radio emission observed by Neff & Hutchings (1992) are shown in overlay in Figure 4. Images obtained in the  $H$  and  $J$  bands are shown in Figures 5 and 6. A near-infrared circumnuclear structure approximately  $6''$  (1.6 kpc) in diameter is clearly visible; however, Figures 3–6 indicate that the spatial distribution of the emission varies strongly as a function of the observed wavelength. At  $2.2 \mu\text{m}$ , a clumpy ring-like structure surrounds the nucleus of NGC 7771. Although still visible, the  $2.2 \mu\text{m}$  emitting clusters are less pronounced at  $1.65 \mu\text{m}$ . The circumnuclear morphology at  $1.25 \mu\text{m}$  is clearly dominated by the southeastern ridge of knots. With the exception of this ridge, the remaining clumps have faded into the diffuse background light of the galaxy. On the basis of the differential morphology observed in the  $J$  through  $K$  bands, we suspect that many of the knots comprising the ring are obscured at shorter wavelengths. The  $I$  band image shown in Figure 1 and the other optical images referred to in Section 1 do not possess sufficient spatial resolution to test this hypothesis. This issue will be discussed further in Section 4.2. The  $JHK$  behavior of this starburst ring may be contrasted with that of the ring in the luminous starburst + Seyfert 1 galaxy NGC 7469, in which the emission becomes progressively smoother from the  $J$  to  $K$  bands (Genzel et al. 1995).

The data indicate that the relative intensities of the knots at near-infrared and radio wavelengths are variable. For example, the brightest region in the  $K$  band is the linear ridge of emission (knots Kf – Kh); the brightest knot at 6 cm is the westernmost knot (Ra). Furthermore, the clumps that are prominent at  $2.2 \mu\text{m}$  are *not* spatially coincident with those observed at 6 cm and appear to be nearly perfectly anti-correlated with the radio emitting features. The distribution of the  $K$  band knots appears to follow an ellipse with semi-major and semi-minor axes of  $a = 2.62''$  and  $b = 1.25''$ , respectively, at  $\text{PA} \approx 90^\circ$ . The apparent axis ratio of the  $K$  band ring is  $q(K) = b/a = 0.48$ . The distribution of the radio clumps can be described in terms of a similar ellipse ( $a = 2.75''$ ,  $b = 1.25''$ ,  $q(6\text{cm}) = 0.45$ ) whose semi-major axis lies at  $\text{PA} \approx 73^\circ$ . The data have been carefully examined for instrumental effects and alignment effects, and we conclude that this anti-correlation is in fact real.

To assess the intrinsic structure of the rings, we have deprojected the ellipses defined by the near-infrared and the radio emitting knots (e.g. Buta 1986a; Buta 1986b; Buta 1990; Buta & Purcell 1998). The results of the deprojections should be regarded with caution since the inherent assumption of coplanar orbits may not be valid in an interacting system. The situation is further

complicated by the high inclination angle and the uncertainty in the inclination angle. Osman (1986) derives an inclination angle of  $i = 66^\circ \pm 3^\circ$  from the outer ( $60'' \lesssim r \lesssim 96''$ ) isophotes of a blue photograph of NGC 7771. Using a Gunn *r* image, Nordgren et al. (1997) find a value of  $i = 75^\circ \pm 4^\circ$ . Ellipse fitting to the *I* band image shown in Figure 1 reveals that the distorted morphology of NGC 7771 is at least partly responsible for this large range of values. The *I* band data show the presence of a bright elongated structure between radii of  $20'' \lesssim r \lesssim 40''$  with  $P.A. \sim 77^\circ$  and a more circular outer disk with  $P.A. \sim 67^\circ$ . Ellipse fitting at radii  $r \gtrsim 80''$  becomes unreliable, as the observed material is contaminated by tidal features. We adopt an inclination angle of  $i = 69^\circ \pm 6^\circ$ , based upon the ellipticity of the *I* band isophotes in the relatively undisturbed region located between  $38'' \lesssim r \lesssim 75''$ , and an assumed intrinsic axial ratio of 0.2. This value of the inclination angle is intermediate between those of Osman (1986) and Nordgren et al. (1997). The implied intrinsic axis ratios are  $q_0(K) = 0.71$  and  $q_0(6\text{cm}) = 0.68$ . We note that the intrinsic axis ratios could be as round as  $q_0(K) = 0.85$  and  $q_0(6\text{cm}) = 0.88$  if  $i = 66^\circ$ , and as oblate as  $q_0(K) = 0.54$  and  $q_0(6\text{cm}) = 0.52$  if  $i = 75^\circ$ . The large uncertainty in the intrinsic shapes of the rings reflects the difficulties of assessing the intrinsic structure of a highly inclined, interacting system. The intrinsic major axis of the nuclear *K* band ring is aligned with that of the radio ring to within  $5^\circ$  for all three inclination angles, i.e. the displacement between the major axes of the near-infrared and the radio rings is largely a projection effect. The locations of the individual near-infrared and radio emitting knots remain anti-correlated after deprojection, however. Finally, we note that the deprojections suggest that the rings lead the bar by an intrinsic angle  $\Theta_{Br} \sim 35^\circ - 55^\circ$ , depending upon the adopted inclination angle and bar position angle.

The weakness or absence of radio emission at the locations of near-infrared or visual emission peaks has also been noted in M 82 and in NGC 253 (Sams et al. 1994; Golla, Allen, & Kronberg 1996; Ulvestad & Antonucci 1997). We note that the distribution of the *H* – *K*, *J* – *H*, and *J* – *K* colors in NGC 7771 follows that of the *K* band emission, i.e. the reddest regions are spatially coincident with the *K* band peaks, and not the radio peaks. In contrast, the reddest *J* – *K* colors in NGC 253 and in the starburst ring in NGC 7469 are found at the locations of the 6 cm emission peaks (Sams et al. 1994; Genzel et al. 1995).

### 3.2. Photometry and Colors

The redshift-corrected *J*, *H*, and *K* band fluxes of the near-infrared luminous knots identified in Figure 3 and the nucleus (denoted N) are given in Table 1. The  $1\sigma$  uncertainty in the fluxes is typically 8% at *K*, 5% at *H*, and 6% at *J*. These data indicate that the starburst complexes are extremely active, with fluxes equaling  $\approx 50\%$  that of the nucleus. The 6 cm fluxes of the radio-bright knots are quoted in Table 2. These fluxes represent lower limits and are not corrected for redshift due to the lack of information concerning the spectral energy distribution of the knots in the radio.

The near-infrared *J* – *H* and *H* – *K* colors of knots Ka–Kj and the nucleus are compiled in

Table 1 and plotted in Figure 7. These colors are not dependent upon the alignment of the  $J$ ,  $H$  and  $K$  band images since they represent quantities integrated over an aperture size significantly larger than any uncertainties in the image alignment. The colors range from  $H - K = 0.53 \pm 0.11$  mag and  $J - H = 0.91 \pm 0.07$  mag at knot Kg to  $H - K = 0.72 \pm 0.10$  and  $J - H = 1.13 \pm 0.07$  mag at the nucleus. As discussed in Section 2, the uncertainty in the  $H - K$  color is likely to be overestimated. The *relative* colors of the knots are much better determined than the absolute colors since the quoted uncertainties are determined by the flux calibration, and not by statistical uncertainties. Thus, Figure 7 indicates that knots Kf, Kg, and Kh are the bluest sources, and knots Ka, Kb, Kc, and Ki, along with the nucleus (N), are the reddest sources.

Standard “mixing” curves for the CIT photometric system are also shown in Figure 7 to illustrate the effects of emission from blue stars, thermal gas, synchrotron emission, and hot dust upon the near-infrared colors of “normal” stellar populations (Paper 2; Paper 3; Joseph et al. 1984; Telesco et al. 1991a; Turner et al. 1992). The colors of “normal” stellar populations are taken to be  $H - K = 0.18$  and  $J - H = 0.71$  mag, which correspond to the colors of red giants (Turner et al. 1991; Frogel et al. 1978). Red supergiants, which are important energy sources in starbursts that are  $\sim 10$  Myr old, are very similar in color. The dotted line delineates the region of the color-color diagram that can be reached by existing reddening models (Gordon, Calzetti, & Witt 1997; see also Paper 3). These models employ both Galactic and Small Magellanic Cloud (SMC) extinction laws and consider both homogeneous and clumpy dust distributions. The reddening vectors for an overlying dust screen, a sphere of uniformly mixed dust and stars, and a dust-free sphere of stars surrounded by a clumpy shell of dust are shown as examples. Figure 7 indicates that the colors of many of the knots are redder than those of an unobscured “normal” stellar population, and are marginally redder than those of a heavily obscured “normal” stellar population.

#### 4. The History of Star Formation in NGC 7771

In the sections below, we discuss the current dataset with the goal of providing *plausible* constraints upon the history of star formation in NGC 7771 and encouraging further observations of this system. We note that the existing dataset for NGC 7771 is not yet comprehensive enough to permit detailed modeling of the star formation history, as performed for NGC 7469 by Genzel et al. (1995) and references therein.

##### 4.1. The Nature of the Radio Emission

Compact radio sources have been detected in several nearby star forming galaxies including M 82, NGC 253, NGC 4736, and NGC 7469 (Kronberg, Biermann, & Schwab 1985; Ulvestad & Antonucci 1997, and references therein; Duric & Dittmar 1988; Wilson et al. 1991). The radio

emission from M 82 has been interpreted in terms of supernovae remnants surrounded by dense shells (Kronberg et al. 1985; Golla et al. 1996). Approximately half of the sources in NGC 253 and in NGC 4736 are thermal sources associated with HII regions; the remaining sources are non-thermal supernovae remnants (Duric & Dittmar 1988; Ulvestad & Antonucci 1997). The radio emission associated with the ring in NGC 7469 is non-thermal in nature (Wilson et al. 1991). Based upon observations of other starburst systems, it is not clear whether the emission from the radio sources in NGC 7771 is expected to be thermal or non-thermal in nature. The fact that the starburst ring is not detected at 2 cm (Batuski & Hanisch, private communication) does not resolve this issue since the 2 cm fluxes predicted for individual knots assuming either thermal or non-thermal spectral indices ( $S_\nu \propto \nu^{-\alpha}$ ) are below the detection limits of Batuski et al. (1992).

To provide some insight into the relative importance of thermal and non-thermal emission processes in NGC 7771, we consider the simple case in which the radio emission is optically thin and the spatial variations in the spectral index are not severe. The global 6 cm and 20 cm flux measurements of Condon et al. (1991) then place some constraints upon the relative roles of thermal and non-thermal emission in NGC 7771. These authors find a global 6 cm flux of 60 mJy and a spectral index of  $\alpha = 0.62$ . Emission from NGC 7770 accounts for 10% of the total flux (Condon et al. 1991). These data imply that 24.8 mJy (46%) of the global total 6 cm emission from NGC 7771 is thermal emission, assuming that the thermal and non-thermal components of the radio emission are characterized by spectral indices of  $\alpha = 0.1$  and  $\alpha = 0.9$ , respectively (e.g. Mas-Hesse & Kunth 1991). For comparison, the data obtained by Neff & Hutchings (1992) (Figure 2) show that the total 6 cm flux associated with the starburst ring, as measured by an outer ellipse characterized by  $a = 3.88''$  and  $b = 1.88''$  at  $PA = 73^\circ$  and an inner ellipse with  $a = 1.25''$  and  $b = 0.58''$  at  $PA = 84^\circ$ , is 29.4 mJy. The flux from the region interior to the inner ellipse, which is dominated by the nucleus, amounts to 4.2 mJy. The remaining 20.4 mJy of the total 54 mJy associated with NGC 7771 lies outside of the central 2 kpc. These data are summarized in Table 3.

Given that NGC 7771 emits a global thermal flux of 24.8 mJy and that the total thermal + non-thermal flux associated with the ring is 29.4 mJy, it is conceivable that all of the thermal emission is produced by the ring. The  $H\alpha$  profile in Keel (1996) suggests that some of the thermal emission must reside in the disk of NGC 7771, however. To provide a plausible constraint upon the emission properties of the central 2 kpc of NGC 7771, we assume that the emission properties of the disk are similar to those observed in “normal” star forming galaxies, in which  $\approx 20\%$  of the global 6 cm emission is thermal and the spectral index is  $\alpha \approx 0.8$  (e.g. Condon 1992, and references therein). Consequently, 4.1 mJy of the 20.4 mJy of 6 cm emission lying outside of the central 2 kpc will be thermal. This leaves 20.7 mJy of thermal flux lying within the starburst ring and the nucleus. That is, 62% of the 6 cm emission associated with the ring and the nucleus is thermal emission. The implied average spectral index for the ring and the nucleus is  $\alpha = 0.50$ . For comparison, the disk can produce at most 20.4 mJy of the total thermal flux. The average spectral index for the central 2 kpc would be  $\alpha = 0.83$  in the case where the ring and the nucleus



produce the remaining 4.4 mJy of thermal flux, as summarized in Table 3.

The average spectral indices can be compared to those illustrated by Mas–Hesse & Kunth (1991), hereafter MHK91, (their Figure 17) and tabulated by Cerviño & Mas–Hesse (1994), hereafter CMH94. These authors model several starburst parameters for the cases of an instantaneous burst of star formation (ISB) and a burst with a constant star formation rate (CSFR). We adopt the CMH94 models since they track the time evolution of a larger number of radio parameters than other models in the literature (e.g. Bruzual & Charlot 1993; Leitherer & Heckman 1995, and references therein). The CMH94 models referred to in the remainder of this paper employ a Salpeter initial mass function (IMF) with lower and upper mass cutoffs of  $2 M_{\odot}$  and  $120 M_{\odot}$ , respectively, and are for solar metallicity. The reader is referred to CMH94 for additional data from models utilizing different IMF slopes and metallicities. Illustrations for earlier versions of the model may be found in MHK91. We emphasize that the case of a Salpeter IMF with solar metallicity is chosen solely to illustrate the *general* behavior of a starburst. The exact details of the time evolution of the starburst occurring in NGC 7771 may differ from that discussed here, depending upon the exact form of the IMF and the metallicity.

The CMH94 models indicate that a spectral index of  $\alpha = 0.50$  is matched by a 4 to 5 Myr old instantaneous burst. A value of  $\alpha = 0.83$ , which is similar to that of the starburst ring in NGC 7469 (Wilson et al. 1991), corresponds to an 8 Myr old instantaneous burst. A constant star formation rate appears to be inconsistent with the data since the CMH94 models indicate that the maximum value reached in the CSFR model considered here is  $\alpha \sim 0.3$ . The radio data thus indicate that the activity occurring in the central 2 kpc of NGC 7771 can be explained in terms of an instantaneous burst of star formation which occurred 4 to 8 Myr ago, assuming that the observed radio emission is optically thin. Deep 2 cm mapping, combined with the existing 6 cm data, would place stronger constraints upon the star formation history of the radio–bright knots.

## 4.2. The Extinction towards the Ionized Gas

The optical measurements of the central  $0.55 \times 2$  kpc of NGC 7771 by Veilleux et al. (1995) confirm that the ionized gas in NGC 7771 is heavily obscured. Veilleux et al. (1995) observe an H $\alpha$  flux of  $F(\text{H}\alpha) = 5.9 \times 10^{-14}$  ergs s $^{-1}$  cm $^{-2}$  and an H $\alpha$ /H $\beta$  line ratio of  $F(\text{H}\alpha)/F(\text{H}\beta) = 21.4$ , whereas standard recombination line theory predicts  $F(\text{H}\alpha)/F(\text{H}\beta) = 2.85$ . These data imply  $A_V = 5.2$  mag for an overlying screen of non–scattering dust which obeys the extinction law of Whittet (1992) as quoted by Gordon et al. (1997) (their Table 1). In this case, the observed H $\alpha$  flux corresponds to 2% of the intrinsic H $\alpha$  flux.

The observed H $\alpha$  flux can also be compared to that predicted from the thermal radio flux following standard recombination theory (e.g. Condon 1992):

$$F(\text{H}\alpha) = 0.80 \times 10^{-12} \left( \frac{T_e}{10^4 \text{K}} \right)^{-0.52} \left( \frac{\nu}{\text{GHz}} \right)^{0.1} \left( \frac{S_T}{\text{mJy}} \right) \text{ergs s}^{-1} \text{cm}^{-2} \quad (1)$$

where  $T_e$  is the electron temperature, and  $S_T$  is the thermal radio flux. An electron temperature of  $T_e \sim 10^4$  K is assumed. The total 6 cm flux measured in the central  $0.55 \times 2$  kpc is 28.2 mJy. In the case that the spectral index of the radio emission is  $\alpha = 0.50$  (Section 4.1), a total of 17.5 mJy of the flux lying within the slit is thermal. The corresponding H $\alpha$  flux is  $1.64 \times 10^{-11}$  ergs s $^{-1}$  cm $^{-2}$ . This implies that the observed H $\alpha$  flux is 0.4% of the intrinsic H $\alpha$  flux, i.e. that the extinction is  $A_V = 7.9$  mag. If  $\alpha = 0.83$ , the extinction is  $A_V = 6.0$  mag. The H $\alpha$ , H $\beta$ , and 6 cm data thus indicate that the optical depth is between  $A_V = 5$  and  $A_V = 8$  mag, in the case that the dust can be modeled by an non-scattering overlying screen of material of Galactic composition. The relatively narrow range of extinction values suggests that optical recombination lines provide a reasonably accurate measurement of the *average* optical depth, i.e. that the average effects of differential extinction are not severe.

We note that the intrinsic H $\alpha$  flux predicted from the thermal radio flux appears to exceed that predicted from the H $\alpha$ /H $\beta$  line ratio by a factor of 2 to 5, depending upon the exact value of the thermal flux. This discrepancy may simply reflect the inherent uncertainties involved in synthesizing the radio flux contained within the slit used for the optical observations. Alternatively, the difference in the fluxes may indicate that some of the starburst knots are so heavily obscured that none of the H $\alpha$  emission can escape. This hypothesis seems reasonable since the H $\alpha$ /H $\beta$  line ratio indicates that only 2% of the H $\alpha$  emission escapes from the central 2 kpc, i.e. that the starburst is heavily obscured, and could be easily verified by high resolution recombination line imagery. Additional evidence supporting the presence of heavy extinction lies in the *JHK* continuum emission and the H $\alpha$  rotation curve, as discussed in Sections 3.1, 4.3 and 5.

Finally, a comparison between the observed and the theoretical H $\alpha$ /H $\beta$  line ratios and the extinction models of Gordon et al. (1997) reveals that the dust must lie largely in front of the ionized gas. Similar results are found for the samples of starbursts studied by Gordon et al. (1997) and by Meurer et al. (1995), and for M82 (Satyapal et al. 1997). In the case of NGC 7771, none of the Gordon et al. (1997) models incorporating uniformly mixed dust and stars are able to produce an H $\alpha$ /H $\beta$  line ratio as high as 21.4. The only models which are capable of producing line ratios of this magnitude involve a sphere of stars surrounded by a shell of homogenous dust, and a sphere of stars surrounded by a shell of slightly clumpy dust. In the clumpy case, the ratio of the interclump to clump medium density ratio is  $k_2/k_1 = 0.1$  in the terminology of Gordon et al. (1997). That is, the clumps are ten times denser than the interclump regions. This model is the least clumpy of the models considered by Gordon et al. (1997). Since our goal is to construct a plausible scenario which can explain the available data, we adopt the simplest case in the remainder of the paper: an overlying non-scattering dust screen and an average extinction of  $A_V = 6.5$  mag. The relationship between the extinction towards the ionized gas and the continuum sources will be examined in the next section.

### 4.3. The Near-Infrared Continuum Emission

The near-infrared colors of the starburst knots and of the nucleus are significantly redder than those of an unobscured population of evolved red stars, as discussed in Section 3.2. Such deviations are well-documented in the literature (Paper 2; Paper 3; Carico et al. 1988; Devereux 1989; Joseph et al. 1984) and can reflect the presence of very large amounts of dust, as well as emission sources other than evolved red stars. The roles of synchrotron processes, blue stars, thermal gas associated with HII regions, and hot dust in determining the near-infrared colors of starburst systems have been discussed by several authors. Synchrotron radiation accounts for a negligible portion of the near-infrared emission (Paper 1; Paper 3). Emission from blue stars typically produces as little as  $< 1\%$ , and as much as  $\approx 30\%$ , of the  $K$  band light emitted by starbursts (Satyapal et al. 1997; Paper 3). Contributions from thermal gas emission are only a few percent in many cases (Satyapal et al. 1997; Paper 3). The role of emission from hot dust is somewhat controversial. For example, Lester et al. (1990) and Larkin et al. (1994) find that hot dust emission plays an important role in certain regions of M 82. McLeod et al. (1993) and Telesco et al. (1991b) argue against large amounts of hot dust emission, however.

We therefore expect the intrinsic colors of the starburst knots to be consistent with those of a stellar population containing evolved red stars, with small to moderate contributions from emission from blue stars, thermal gas and hot dust. Figure 8 shows the near-infrared colors of the region covered by the slit ( $H - K = 0.57$  mag,  $J - H = 0.96$  mag) used by Veilleux et al. (1995), corrected for an average  $A_V = 6.5$  mag of extinction. A non-scattering overlying dust screen and the extinction law of Whittet (1992) are used, as discussed above. Figure 8 suggests that the intrinsic colors of the region covered the slit require a *large* fraction ( $\sim 50 - 60\%$ ) of the  $2 \mu\text{m}$  light be produced by blue OBA stars. The contributions from thermal gas and from hot dust do appear to be very small ( $\lesssim 10\%$ ). To test the validity of this result, we now discuss the available evidence concerning each of the possible near-infrared emission mechanisms.

#### 4.3.1. Red Giants and Red Supergiants

The central luminosity of NGC 7771 implies that emission from the underlying stellar population, i.e. old red giants, is negligible. The bulges of “normal” galaxies, whose near-infrared emission is powered by red giants, are characterized by masses of  $\sim 10^9 M_\odot$  and  $K$  band mass-to-light ratios of  $M/L_K = 0.7 M_\odot/L_{K,\odot}$  (Devereux 1989; Devereux, Becklin, & Scoville 1987; Thronson & Greenhouse 1988). This implies that an underlying stellar population of mass  $\sim 10^9 M_\odot$  should have an absolute  $K$  band magnitude of  $M_K = -18.7$  mag, where  $M_{K,\odot} = 3.39$  (Devereux 1989). The absolute magnitude of the central  $10''$  (2.7 kpc) of NGC 7771 is  $M_K = -23.7$  mag (Paper 2). Thus, red giants due to a “normal” old bulge population can power only 1% of the  $K$  band flux associated with this region.

Red supergiants are a likely source of the large luminosity enhancement due to their low

temperatures and high luminosities (e.g. Devereux 1989). For example,  $M_K = -10.8$  mag for a K4 I star,  $M_K = -5.0$  mag for an O4 V star, and  $M_K = 0.6$  mag for an A0 V star (Koornneef 1983; Schmidt–Kaler 1982; Doyon, Joseph, & Wright 1994). MHK91 (their Figure 8a) and CMH94 follow the  $2 \mu\text{m}$  monochromatic luminosity as a function of time for an instantaneous burst of star formation (ISB) and a burst with a constant star formation rate (CSFR). The fractional contributions of emission from red supergiants and nebular emission to the  $2 \mu\text{m}$  continuum emission calculated by CMH94 are shown in our Figure 9. The percentage of emission that is not produced by red supergiants (RSGs) or by nebular emission is also indicated. While the general trends predicted by these models should be valid, the details should be regarded with some caution as the evolutionary behavior of red supergiants is uncertain (Leitherer & Heckman 1995; Lançon & Rocca–Volmerange 1996). The very first red supergiants begin to appear 3 to 4 Myr after the onset of star formation and become numerous when the burst is  $\sim 10$  Myr old. The models show that red supergiants produce a strong enhancement in the  $K$  band luminosity when the starburst is  $\approx 10$  Myr old. In an instantaneous burst, the luminosity enhancement quickly fades as the red supergiants die. The  $K$  band luminosity of a CSFR starburst continues to rise during the first 20 Myr as more stars reach the red supergiant stage.

Evidence supporting the presence of red supergiants in NGC 7771 is also found in the  $K$  band spectrum discussed in Paper 2 and Paper 3. The photometric CO index measured in the central  $3.0'' \times 2.5''$  ( $CO_{ph} > 0.18 \pm 0.02$  mag) indicates that the CO bandheads in this region are stronger than those of “normal” galaxies. The most likely explanation for the presence of the strong CO absorption features is the existence of a population of young red supergiants (Paper 3; Doyon, Joseph, & Wright 1994; Goldader et al. 1997; Rieke et al. 1993). We note that the spectrum presented in Paper 2 probably contains light from both the nucleus and the starburst ring due to the size of the extraction aperture ( $3.0'' \times 2.5''$ ) and the seeing conditions. Examination of the complete dataset indicates that the strong CO absorption features are present throughout the central  $6.0'' \times 2.5''$  of NGC 7771. We therefore conclude that starburst ring contains red supergiants. In this case, the star formation activity in the near–infrared bright regions must be  $\gtrsim 4$  Myr old, and is likely to be  $\sim 10$  Myr old (CMH94; Leitherer & Heckman 1995; see also Section 6). The observed photometric CO index and the models of Doyon et al. (1994) and Satyapal et al. (1997) are in fact consistent with an  $\approx 10$  Myr old burst.

#### 4.3.2. Nebular Emission

The amount of near–infrared emission from thermal gas and from blue stars is best constrained by maps of the  $\text{Pa}\beta$  or  $\text{Br}\gamma$  recombination lines. In the case of NGC 7771, such data are not available for the individual knots which comprise the starburst ring. The fact that the near–infrared bright knots are not radio–bright does suggest that emission from thermal gas will not make a significant contribution to their  $2 \mu\text{m}$  luminosities, however. The  $\text{H}\alpha$  flux measured by Veilleux et al. (1995) may be used to investigate this hypothesis. We assume standard case B

recombination theory, in which case the ratio of the Br $\gamma$  and H $\alpha$  line fluxes is Br $\gamma$ /H $\alpha$  = 0.0098 for an electron temperature of  $T_e = 10^4$ K. As in Section 4.2, the extinction is modeled as a non-scattering overlying screen of Galactic composition with  $A_V = 6.5$  mag. The total Br $\gamma$  flux observed in the central 2 kpc should then be  $3.3 \times 10^{-14}$  ergs s $^{-1}$  cm $^{-2}$ . The relationships given in Satyapal et al. (1995) or in Paper 3 can then be used to predict the amount of thermal gas emission observed at 2  $\mu$ m. We find that emission from thermal gas produces  $\sim 3\%$  of the total 2  $\mu$ m continuum emission associated with the central 2 kpc of NGC 7771. In the case where the extinction is as high as  $A_V = 7.9$  mag or the electron temperature is as high as  $T_e = 20000$ K, thermal gas emission still produces less than 20% of the  $K$  band emission in this region.

#### 4.3.3. Blue Stars

The CMH94 models can also be used to constrain the fractional amount of 2  $\mu$ m emission produced by blue stars. As indicated in Figure 9, the CMH94 CSFR model suggests that the maximum contribution to the 2  $\mu$ m luminosity from sources other than red supergiants and nebular emission is  $\sim 25\%$ . Consequently, a CSFR burst appears to be inconsistent with the extinction-corrected near-infrared colors, which predict a  $\sim 50 - 60\%$  contribution from nebular emission (Figure 8). The ISB model indicates that stars other than RSGs produce a large fraction (35 to 60%) of the  $K$  band emission only at burst ages between  $\sim 3$  and 4 Myr, before emission from red supergiants is significant, and at 20 Myr, when the red supergiants are dying. These ages seem unlikely based upon the evidence supporting the presence of RSGs. Furthermore, the contribution from nebular emission is large (60 to 20%) between ages of 3 and 4 Myr. An older burst ( $> 20$  Myr old) also appears to be ruled out by the extinction-corrected  $J - K$  color of the region covered by Veilleux et al.'s slit ( $J - K = 0.33$  mag), which is significantly bluer than that of a 20 Myr old ISB ( $J - K = 0.67$  mag). Use of an attenuation model incorporating different dust geometries and scattering increases the agreement between the data and the models by only a marginal amount. The resolution of this problem is discussed in Section 4.3.5.

#### 4.3.4. Hot Dust

Information regarding the role of hot dust is provided by the  $K - L'$  color measurements of Carico et al. (1988). These authors find a color of  $K - L' = 0.79$  mag, corrected for redshift, for the central 5'' (1.4 kpc) of NGC 7771. Colors of  $K - L' > 0.66$  mag indicate the presence of hot dust emission (Joseph et al. 1984). Our  $K$  band image indicates that the near-infrared emission from the central 5'' is dominated by the starburst ring. The  $K - L'$  color is therefore assumed to be associated with the starburst ring. The amount of dust emission in this region can be loosely constrained by comparing the  $J - H$  and  $K - L'$  colors to color-color plots such as those found in Larkin et al. (1994). Taking the average of the  $J - H$  colors quoted in Carico et al. (1988) and in Paper 2, the colors of  $J - H = 0.88$  and  $K - L' = 0.79$  imply that not more than  $\approx 20\%$  of the  $K$

band emission can be produced by dust at temperatures of 800 K. This figure drops to  $\lesssim 5\%$  if the temperature of the emitting dust is 500 K. Dust temperatures of 1000 K do not appear to be consistent with the observed colors.

#### 4.3.5. *The Extinction towards the Continuum Sources*

With the caveat that the apparent discrepancies between the models and the observations may simply reflect the uncertainties in modeling the near-infrared portion of the starburst spectral energy distribution, we suggest that an extinction correction based upon the  $H\alpha$  emission is not appropriate for the near-infrared bright knots. Calzetti, Kinney, & Storchi-Bergmann (1994) have found that the optical depths derived from recombination lines and from UV/optical continuum measurements differ by a factor of  $\sim 2$  in UV-bright starbursts. The discrepancy in the optical depths implies different covering factors for the stars producing the continuum emission and for the ionized gas (Calzetti 1997). This effect may also be present at near-infrared wavelengths, but is not well-constrained (Calzetti, private communication).

The relative spatial distributions of the  $K$  band and the 6 cm emission may provide the best insight into this issue. Thermal radio emission should be associated with the sources responsible for the observed  $H\alpha$  emission. The fact that the radio-bright knots are not spatially coincident with the near-infrared bright knots may indicate that the recombination line emission is not associated with the near-infrared sources. Recombination line images or radio spectral index maps are needed to confirm this hypothesis (see also Section 4.1).

We conclude that the optical depth towards the near-infrared sources differs from the optical depth towards the ionized gas. If the optical depth towards the near-infrared knots is one-half that towards the ionized gas, i.e.  $A_V = 3.25$  mag, the extinction corrected colors of the region covered by the slit will be  $H - K = 0.34$  and  $J - H = 0.59$  mag. These colors are consistent with emission dominated by red stars, with small contributions from blue stars and thermal gas a contribution from 800 K dust of  $\leq 20\%$ , as predicted by the observations and models. In this scenario, the reddest near-infrared colors are associated with the near-infrared continuum sources instead of the ionized gas because the combined effect of their intrinsically red color and optical depth is redder than that of the heavily obscured, but intrinsically blue HII regions.

The geometry of the obscuring dust associated with the near-infrared knots may also differ from that affecting the gas, i.e. the dust may not be well-represented by an overlying screen. Figure 7 suggests that the near-infrared colors of the individual knots could easily be explained in terms of emission from a heavily obscured population of red stars, with small contributions from hot dust, blue stars, and thermal gas, if the dust is distributed in a sphere or clumpy shell. For example, the colors are consistent with those of emission dominated by red stars, with 5 – 10% contributions from blue stars, thermal gas, and hot dust and optical depths ranging from  $A_V \sim 10$  to 30 mag, where the dust and stars are uniformly mixed and spherically distributed.

The differential morphology of the starburst ring at  $J$ ,  $H$ , and  $K$  can then be understood in terms of a combination of effects from extinction and possibly hot dust. Assuming that the CMH94 models reproduce the general behavior of a starburst, the 1.2 to 2.2  $\mu\text{m}$  emission from a system with little near-infrared nebular emission should be dominated by red supergiants. The morphologies in the  $J$ ,  $H$ , and  $K$  bands should therefore be similar. The fact that the starburst ring is best seen at the longest wavelengths, where the optical depth is  $\approx 10$  times lower than in the visual, suggests that extinction effects play a major role in determining the morphology of this object and that the starburst knots are heavily obscured. The southeastern portion of the ring appears to be less heavily obscured than the western portion (compare Figures 4 and 6, Table 1 and Figure 7). Emission from hot dust, whose effects will be strongest in the  $K$  band, may play an additional role in highlighting the starburst complexes at 2.2  $\mu\text{m}$ . The ages of the individual knots cannot be determined from the existing data, but are likely to be  $\approx 10$  Myr, based upon stellar population models.

#### 4.4. Stellar Populations

The results of the previous sections can be used to loosely constrain the stellar content and the supernovae rate of the individual knots comprising the starburst ring. In the following discussion, we assume that the radio-bright knots are optically thin, 4 Myr old, and characterized by a spectral index of  $\alpha = 0.50$ . In the case that the spectral index is  $\alpha = 0.83$ , quantities derived from the thermal and non-thermal radio fluxes would be lowered and raised by a factors of  $\approx 5$  and  $\approx 2$ , respectively. The age of the near-infrared bright knots is taken to be 10 Myr old. Extinction is clearly an issue for these knots. However, the optical depths towards the individual knots cannot be uniquely determined since the geometry of the obscuring dust and the intrinsic colors of the knots are not well-determined. We assume an average optical depth of  $A_V = 3.25$  mag ( $A_K = 0.3$  mag). The fraction of the  $J$ ,  $H$ , and  $K$  band emission escaping from an individual knot will then be 43%, 60%, and 75%, respectively. For comparison, if we assume optical depths ranging from  $A_V = 10$  to  $A_V = 30$  mag for a spherical, uniform distribution of dust and stars, 16 to 42%, 25 to 56%, and 40 to 71% of the  $J$ ,  $H$ , and  $K$  band emission, respectively, will escape. Quantities derived from the extinction-corrected  $K$  band fluxes using  $A_V = 3.25$  are therefore likely to represent lower limits and are probably accurate to within a factor of  $\approx 2$ .

##### 4.4.1. Ionizing Stars and Supernovae Remnants

For a spectral index of  $\alpha = 0.50$ , 62% of the total 6 cm flux will be thermal. The radio fluxes listed in Table 2 can then be converted to an ionization rate,  $N_{UV}$ , and a supernovae rate,  $\nu_{SN}$ .

The number of ionizing photons emitted per second (the ionization rate) is derived from

standard recombination theory:

$$N_{UV}(\text{s}^{-1}) = 7.1 \times 10^{49} \left( \frac{D}{1\text{Mpc}} \right)^2 \left( \frac{\nu}{\text{GHz}} \right)^{0.1} \left( \frac{T_e}{10^4\text{K}} \right)^{-0.76} S_T(\nu) \quad (2)$$

where  $S_T(\nu)$  is the thermal radio flux in mJy, and  $T_e$  is the electron temperature. We assume a value of  $T_e = 10000\text{K}$ . The resulting values of  $N_{UV}$  are given in Table 6. For comparison, the numbers of O6 stars that would reproduce the quoted values of  $N_{UV}$  are also quoted, where  $\log N_{UV} = 49.08$  for an O6 star (Panagia 1973.) On average, each radio–luminous knot produces an ionizing flux which is equivalent to that of 35000 O6 stars ( $\log N_{UV} = 53.63$ ).

The supernovae rate is derived following Condon & Yin (1990):

$$L_{NT}(\text{WHz}^{-1}) \sim 1.3 \times 10^{23} \left( \frac{\nu}{1\text{GHz}} \right)^{-\alpha} \nu_{\text{SN}}(\text{yr}^{-1}), \quad (3)$$

where  $L_{NT}$  is the non–thermal radio luminosity and  $\alpha \sim 0.8$  is the non–thermal spectral index. The resulting supernovae rates are compiled in Table 5. On average, each radio–bright knot produces supernovae at a rate of  $\nu_{\text{SN}} = 0.010 \text{ yr}^{-1}$ . The emission from the radio–bright knots is also compared to that of the supernova candidates in M 82 discussed by Kronberg, Biermann, & Schwab (1985). The most luminous radio source in M 82, 41.9 + 58, is considered separately. This source is thought to be a supernova remnant which is surrounded by a dense shell (Kronberg et al. 1985). We find that the radio–bright starburst knots in NGC 7771 could contain 880 M 82–type radio sources, or 35 41.9 + 58 type sources, on average.

#### 4.4.2. Red Supergiants

The absolute  $K$  band magnitudes, corrected for  $A_V = 3.25$  mag of extinction, are given in Table 4. The average, extinction corrected absolute magnitude of the knots in the starburst ring is  $M_K = -20.12$  mag. The  $K$  band properties of the knots are compared with those of infrared–bright starburst clusters observed in M 82 and with those of K4 supergiants. The M 82 clusters are characterized by an average extinction–corrected absolute magnitude of  $M_K = -17.2$  mag in a 29 pc aperture (Satyapal et al. 1997). For K4 supergiants, we adopt an absolute magnitude of  $M_K = -10.8$  (Doyon, Joseph, & Wright 1994). The data indicate that each of the knots located in the ring could contain 15 M 82–type clusters and 5300 red supergiants, on average.

#### 4.4.3. Cluster Masses

Assuming ages of 4 Myr and 10 Myr for the radio and the near–infrared bright clusters, respectively, the CMH94 models may be used to estimate the masses of the clusters. At an age of 4 Myr, the ionizing flux is  $\log N_{UV} = 46.19$  per  $M_\odot$ . A comparison between this value and



the average ionizing flux of the radio knots implies that the radio knots are characterized by an average mass of  $\sim 3 \times 10^7 M_\odot$ . The  $K$  band luminosity of a 10 Myr old cluster is  $L_K = 4.9 \times 10^{30}$  erg s $^{-1}$  Å $^{-1}$  ( $M_K = -2.52$ ) per  $M_\odot$ . The average mass of the near-infrared bright knots is then  $\sim 1 \times 10^7 M_\odot$ . Keeping in mind the uncertainties inherent in these estimates, we adopt  $\sim 2 \times 10^7 M_\odot$  as the typical mass of the individual sources comprising the radio and near-infrared rings. These masses are comparable to those of star forming sites located in starburst galaxies such as the infrared-luminous merger NGC 3690 and the very blue ringed system NGC 3310 (Meurer et al. 1995; Smith et al. 1996b).

The above discussion implies that the total stellar mass associated with the radio and near-infrared rings is  $\sim 4 \times 10^8 M_\odot$  since each ring contains  $\approx 10$  knots. Both the mass of the ring and the number of knots are consistent with the models of nuclear rings discussed by Elmegreen (1994). The data imply that the time-averaged star formation rate for the ring is  $\sim 40 M_\odot$  yr $^{-1}$ . For comparison, the global star formation rate predicted by the far-infrared luminosity is  $dM/dt \sim 3 \times 10^{-10} L_{IR} = 60 M_\odot$  yr $^{-1}$  for constant star formation over a period of 20 Myr and a solar neighborhood IMF with lower and upper mass cutoffs of 2 and 60  $M_\odot$  (Telesco 1988). These star formation rates are also consistent with the models of Elmegreen (1994), in which a ring containing at least 10% of the gas produces at least 50% of the total star formation.

## 5. The Origin of the Ring

Nuclear rings are generally associated with the presence of one or more inner Lindblad resonances (ILRs) in a barred galaxy (Simkin, Su, & Schwarz 1980; Buta 1986a; Binney & Tremaine 1987; Telesco & Decher 1988; Devereux, Kenney, & Young 1992; Buta & Crocker 1993; Elmegreen 1994; Friedli & Martinet 1997). The rings themselves are typically  $\sim 1$  kpc in diameter, but can be characterized by diameters as small as 0.3 kpc or as large as 4.6 kpc (Buta & Crocker 1993). A newly formed, gaseous nuclear ring will lead the primary bar by  $\sim 45^\circ$  (Simkin et al. 1980; Buta, Purcell, & Crocker 1995, hereafter BPC95). The ILRs correspond to the radii where the pattern speed,  $\Omega_b$ , of the bar equals  $\Omega - \kappa/2$ , where  $\Omega$  is the circular angular velocity and  $\kappa$  is the radial epicyclic frequency. The location of the nuclear ring is generally close to the ILR, at the turnover of the rotation curve (Buta 1988). In the case that both an inner ILR (IILR) and an outer ILR (OILR) are present, the circumnuclear ring forms between the two ILRs and lies closest to the IILR (e.g. Telesco & Decher 1988; Elmegreen 1994).

Given that NGC 7771 is a barred galaxy, the most likely explanation for the existence of a nuclear ring is the presence of one or two ILRs. The intrinsic phase shift between the bar and the nuclear rings ( $\Theta_{Br} \sim 35^\circ - 55^\circ$ ; Section 3.1) is similar to that expected for a recently formed resonance feature. The radio and near-infrared images of NGC 7771 suggest that one or two ILRs should be present near a radius of  $\approx 3''$ , i.e. at the location of the observed ring. The H $\alpha$  rotation curve for NGC 7771 obtained by Keel (1996) is shown in Figure 11, corrected for inclination (Section 3.1). This rotation curve must be analyzed with caution since the H $\alpha$  emission may not

effectively probe the heavily obscured nuclear region. Figure 12 shows the eastern and the western portions of the rotation curve, folded about the center of light. On the eastern side of NGC 7771, the velocity first increases with radius, turns over at a radius of  $r \approx 6''$ , and again increases with radius before leveling off. The western arm generally shows solid-body behavior ( $v(r) \propto r$ ). A turnover is not observed.

To determine whether or not the eastern or the western portions of the H $\alpha$  rotation curve do locate the ILRs, the values of  $\Omega(r) = v(r)/r$  and of  $\Omega(r) - \kappa(r)/2$  derived from a smoothed version of the H $\alpha$  rotation curve are shown in Figure 13. The radius  $r$  is defined relative to the continuum peak. The angular velocity of the bar pattern,  $\Omega_b$ , is identified by assuming that corotation occurs at the eastern end of the large scale bar observed in the optical and near-infrared ( $r \approx 35''$ ) (Benedict, Smith, & Kenney 1996). Placing corotation at a radius equal to 1.2 times the bar radius (Devereux et al. 1992, and references therein) would not affect our analysis since  $\Omega$  is fairly constant in the region  $r > 30''$ . With a corotation radius of  $35''$ , the large scale bar has an angular velocity of  $\Omega_b = 6.4 \text{ km s}^{-1} \text{ arcsec}^{-1}$ , or  $23 \text{ km s}^{-1} \text{ kpc}^{-1}$ .

Figure 13 shows that the value of  $\Omega(r) - \kappa(r)/2$  is approximately zero over a large range of radii, as expected for solid body rotation. We do not see evidence of an ILR in the western portion of the H $\alpha$  rotation curve. On the eastern side of NGC 7771, a solution of  $\Omega_b(r) = \Omega(r) - \kappa(r)/2$  is found at  $r \approx 6''$ , i.e. at the turnover point in the rotation curve. Thus, the only apparent ILR lies *exterior* to the nuclear starburst ring.

As discussed previously, the variations in the *JHK* morphology of NGC 7771 indicate that the central 2 kpc of NGC 7771 is heavily obscured and that the western portion of the ring may be more heavily obscured than the southeastern portion. Consequently, the asymmetric behavior of the eastern and western portions of the H $\alpha$  rotation curve and the absence of a western ILR could result from differential extinction. Strong extinction will result in a slowly rising rotation curve, as seen in the western arm of NGC 7771. The models of Bosma et al. (1992) suggest that the amount of obscuration thought to be present in NGC 7771 ( $A_V \sim 6 \text{ mag}$ ) should not have a strong effect upon the observed rotation curve, however. Furthermore, the fact that the ILR observed in the eastern arm of NGC 7771 lies exterior to the nuclear ring is not easily explained by extinction effects, unless the eastern portion of the ring is completely obscured in the visible. These difficulties may indicate that our measurement of the extinction is too low or that differential extinction is not responsible for the odd behavior of the H $\alpha$  rotation curve. High resolution imaging of the H $\alpha$  emission and/or a rotation curve obtained at longer wavelengths would help resolve this issue.

The rotation curve may also be influenced by the interaction between NGC 7771 and other members of the NGC 7771 Group and/or small-scale non-circular motions. Distortions in the optical morphology of NGC 7771 are visible in Figure 1 and have been noted by several authors (Sections 1 and 3.1). Ellipse fitting shows a clear difference in the position angles of the inner and outer disks (Section 3.1). Therefore, the skewed rotation curve may also indicate that the

observations were obtained at a location slightly offset from the kinematic major axis. This hypothesis cannot be confirmed since the available optical and HI data do not precisely determine the position angle of the kinematic major axis. The apparent discrepancy between the location of the observed ILR and the location of the ring may also reflect the presence of a strong bulge. A bulge/disk decomposition of the *I* band data does not provide a meaningful test of this hypothesis due to the heavy extinction and the distorted morphology.

Finally, Buta & Crocker (1993) and Friedly & Martinet (1997) have pointed out that nuclear rings are also present in galaxies containing both a primary bar and a small-scale nuclear bar. In this case, the corotation radius of the nuclear bar is located near the ILR of the primary bar, and the ring forms near the corotation radius of the nuclear bar. The morphology of the circumnuclear feature may resemble hot-spots, a mini-spiral, or a complete ring depending upon the relative phase of the two bars. The nuclear bar is a transient feature in this scenario. In the case of NGC 7771, the  $H\alpha$  rotation curve does not confirm or rule out the presence of two bars. The *K* band data shown in Figure 3 are suggestive, but not conclusive. A weak, small-scale nuclear bar could run from either knots Kc to Ki or from Ke to Kj. The presence of a nuclear bar will be difficult to confirm or rule out due to NGC 7771’s high inclination. Higher resolution *K* band imagery may be able to provide stronger evidence supporting or refuting the existence of a stellar nuclear bar. High resolution maps of the  $H_2$  and/or CO emission may be able to identify a gaseous nuclear bar. The absence of a nuclear bar would not be surprising, however. Many galaxies, including ESO 565 – 11, do not show evidence of a secondary nuclear bar (Buta & Crocker 1993; BPC95).

The current data provides only weak evidence linking the origin of the nuclear ring to a resonance. Additional high resolution imaging and spectroscopy at both optical and longer wavelengths would clarify several of the issues discussed above. Finally, we note that CO maps have recently led to the identification of gaseous rings ranging from 0.6 kpc to 1.6 kpc in diameter in three ultraluminous merging galaxies Downes & Solomon (1998). If nuclear rings also form during mergers and interactions, the nuclear ring in NGC 7771 may be associated with interaction activity instead of an ILR.

## 6. Sequential Star Formation?

As discussed in Section 3.1, the peaks of the near-infrared and the 6 cm emission in the starburst ring are not spatially coincident. This fact, when coupled with the modeled behavior of a starburst and our estimated ages of the radio and near-infrared bright knots, suggests that the radio and the near-infrared observations are tracing multiple generations of star formation. The model behavior of the  $2\ \mu\text{m}$  and the total (thermal + non-thermal) 6 cm luminosities as a function of time, normalized by the total mass of stars formed since the beginning of the burst, is illustrated by MHK91 (their Figures 8a and 16) and tabulated by CMH94. The time-evolution of the *K* band luminosity is discussed in Section 4.3. The total 6 cm emission from an instantaneous burst

rapidly decreases over the first 10 Myr and then levels off as the emission becomes predominantly non-thermal. In the case of constant star formation, the total 6 cm emission is dominated by thermal emission and remains essentially constant after a sharp increase during the first  $\sim 3$  Myr of the burst. The ratio of the  $2\ \mu\text{m}$  ( $L_K$ ) and the 6 cm ( $L_{6\text{cm}}$ ) luminosities, as derived from the CMH94 models, is plotted in Figure 10. The ratio  $L_K/L_{6\text{cm}}$  increases steadily over the first  $\sim 12$  Myr of a CSFR burst before levelling off. In the case of an instantaneous burst, the ratio  $L_K/L_{6\text{cm}}$  increases rapidly as red supergiants appear. The value of  $L_K/L_{6\text{cm}}$  begins to slowly decrease when the burst is  $\approx 10$  Myr old, as the red supergiants begin to die.

The time-evolution of the near-infrared and radio luminosities suggests that the reason that the near-infrared bright knots are radio-dim (and have a higher value of  $L_K/L_{6\text{cm}}$ ), and vice-versa, is that the radio-luminous knots are not the same age as the near-infrared luminous knots. This hypothesis is consistent with the ages of the knots, as estimated from the spectral index of the radio emission and the CO index (4 to 8 Myr old for the radio knots, and  $\sim 10$  Myr old for the near-infrared knots). While we cannot conclusively rule out the possibility that radio-bright knots are older than the near-infrared-bright knots, the current data and models do suggest that the radio-luminous knots are likely to be younger than the near-infrared-luminous knots. Multiple generations of star formation are also observed in the southern ringed galaxy ESO 565 – 11 (Buta, Purcell, & Crocker 1995, hereafter BPC95).

Different conclusions have been reached in the cases of NGC 253, NGC 7469, and M 82, however. In NGC 253, the reddest  $J - K$  colors are correlated with the radio peaks. The radio peaks are interpreted as obscured HII regions; the near-infrared “peaks” are simply holes in the extinction (Sams et al. 1994). The emission from one of the near-infrared sources has also been discussed in terms of a dust-enshrouded supernovae remnant which has not yet broken out of its optically thick molecular cloud (Kalas & Wynn-Williams 1994). Ulvestad & Antonucci (1997) point out that the lack of thermal radio emission from the brightest optical cluster in NGC 253 could indicate that the free-free emission is absorbed by molecular clouds, or that supernovae winds have cleared the region of thermal gas. In NGC 7469, the anticorrelation of the  $J$  band emission peaks and the 6 cm peaks, as well as the clumpiness of the  $J$  band emission, are again attributed to the distribution of gas and dust (Genzel et al. 1995). Their interpretation is supported by the correlation of the reddest  $J - K$  colors and the non-thermal radio emission. In M 82, several non-thermal radio sources lie behind the central dust lane, and optically bright super star clusters (SSCs) lack radio emission (Golla et al. 1996). These authors suggest that the relative radio and optical morphologies indicate that a large number of massive stars and SSCs are obscured by the central dust lane. The lack of radio emission associated with the optical SSCs may also reflect a lower density in the interstellar medium (ISM) surrounding the SSCs.

These discussions indicate that a dimness or a lack of radio emission at the locations of near-infrared emission peaks can be explained by scenarios other than age variations: 1) the near-infrared peaks may represent holes in the extinction and are not real peaks, 2) the near-infrared sources may be young, dust-enshrouded supernovae, and 3) the near-infrared knots

may represent areas where the density of the ISM is low. The first of these explanations is generally invoked when the reddest  $J - K$  colors correspond to the peaks of the 6 cm emission. This is not the case in NGC 7771; the reddest colors are spatially coincident with the 2  $\mu\text{m}$  peaks. Furthermore, the emission becomes clumpier as the observed wavelength changes from 1.25 to 2.2  $\mu\text{m}$ . This behavior suggests that we are seeing further into the galaxy at 2.2  $\mu\text{m}$  and uncovering the true morphology of the near-infrared emitting sources. The second explanation, based upon the work of Kalas & Wynn-Williams (1994), requires that the energy associated with the supernova be absorbed and re-radiated in the infrared. The near-infrared properties of dust-enshrouded supernovae should therefore be consistent with thermal dust emission. In contrast, the near-infrared colors of the knots in NGC 7771 are consistent with stellar emission, with only small contributions from thermal dust emission. Finally, the third explanation appears to be ruled out in the case of NGC 7771 since the fact that the reddest near-infrared colors are associated with the 2  $\mu\text{m}$  sources suggests that these regions are heavily obscured, i.e. that large amounts of gas and dust (and high ISM densities) are likely to be present.

We conclude that the differences between the spatial distribution of the radio and the near-infrared emission most likely reflect the presence of two different epochs of star formation and not the effects of extinction or variations in the ISM density. The physical reason for the spatial displacement between the current and the previous generations of star formation may be due to the rotation of the ring, propagating star formation, or another physical process. For example, the phase shift between the major axes of the young and the old rings in ESO 565 – 11 has been interpreted in terms of the effects of gravitational torques upon a highly oblate ( $q = 0.55$ ) ring (BPC95, and references therein). Finally, effects from a secondary nuclear bar (if one exists) or the interaction between NGC 7771 and other members within the Group may also be important.

The uncertainties in the intrinsic structure of NGC 7771, the origin of the ring, and the lack of kinematic data do not allow us to further constrain the cause of the spatial displacement between the current and previous generations of star formation. For example, the possible effects of gravitational torques are difficult to assess since the intrinsic ring shapes are not easily deduced in such a highly inclined and disturbed system. The fact that the *intrinsic* major axes of the  $K$  band and the 6 cm rings appear to be in alignment to within  $5^\circ$  suggests that the orientations of the rings are not strongly affected by gravitational torques at this time. This scenario is consistent with the rounder intrinsic axis ratios derived for inclinations of  $i = 66^\circ - 69^\circ$  since gravitational torques will have little effect on nearly circular rings. If the rings are instead very oblate, the alignment may imply that gravitational torques have not had enough time to significantly displace the  $K$  band ring, whose age is  $\approx 10$  Myr (Section 4.3.5).

In summary, the data indicate that radio and near-infrared wavelengths are tracing multiple generations of star formation in NGC 7771. The spatial displacements between the current and the previous sites of star formation are probably due to the rotation of the ring, regardless of its origin, and/or propagating star formation. Other factors such as gravitational torques may also be important. We conclude that the spatial distribution of the radio and near-infrared emission

most likely traces *sequential star formation* associated with a rotating ring or propagating star formation.

## 7. Implications Concerning the Birth of an AGN

The presence of circumnuclear starburst rings in galaxies with and without a Seyfert nucleus raises the question: What is the relationship, if any, between circumnuclear rings and AGN? The means by which an AGN is fueled and triggered remains one of the fundamental questions in astronomy. In order to channel large amounts of gas from the outer portions of a galaxy into the small nuclear region hosting the AGN, large amounts of angular momentum must be removed from the gas. Various authors have proposed that a bar, or a series of nested bars, as the mechanism by which this is accomplished (e.g. Simkin et al. 1980; Shlosman, Frank, & Begelman 1989; Shlosman, Begelman, & Frank 1990). Maiolino et al. (1997) find that Seyfert 2 galaxies are in fact more likely to be characterized by asymmetric morphologies associated with interactions, bars, or disk asymmetries than “normal” galaxies. Friedli & Martinet (1997) also note that a large fraction of the galaxies exhibiting nested bars possess Seyfert nuclei. However, the study of Ho, Filippenko, & Sargent (1997) does not find evidence of a causal relationship between bars and AGN.

The causal relationship between bars and nuclear rings of star formation is also a common topic of discussion in the literature (see Section 5). In barred galaxies containing one or more ILRs, gas first accumulates in a ring near the ILR(s). Gas which is not consumed in the ensuing burst of star formation may be transported into the nucleus by a nuclear bar to fuel an AGN (e.g. Pfenniger & Norman 1990; Shlosman et al. 1989; Shlosman et al. 1990). In barred galaxies without an ILR, the gas is channeled directly to the nucleus and may fuel a nuclear starburst and/or an AGN (e.g. Shlosman et al. 1990; Telesco, Dressel, & Wolstencroft 1993; Friedli & Martinet 1997). The relationship between the presence or absence of an ILR and the formation of circumnuclear rings, and nuclear starbursts and AGN may explain the lack of a correlation between bars and AGN observed by Ho et al. (1997) and the apparent lack of a relationship between rings and AGN observed by Maoz et al. (1996).

While the details of AGN formation are not well understood, it is clear that material must fuel the AGN in some manner. We speculate that the near-infrared morphologies of the rings in NGC 7771 and NGC 7469 may provide a clue regarding the relationship between bars, circumnuclear rings, and AGN. The circumnuclear rings in these galaxies are likely to be associated with ILRs, and may be linked to small-scale nuclear bars (Genzel et al. 1995; Section 5). The rings in NGC 7771 and NGC 7469 are also similar in that they both contain compact regions of intense star formation, with tens of thousands of stars contained within areas  $\sim 100 - 200$  parsecs in diameter (Genzel et al. 1995; Section 4.4). In both cases, the ages of the rings are such that the near-infrared emission should be dominated by red supergiants. However, the  $K$  band image obtained by Genzel et al. (1995) suggests that the circumnuclear  $K$  band emission is generally smoother in NGC 7469 than in NGC 7771. As discussed in this paper, our data suggest that the

clumpiness of the  $K$  band emission from NGC 7771 is not the result of extinction.

The perceived difference in the clumpiness of the  $K$  band emission could be the result of the ages and the sizes of the clusters formed in the rings. While star formation generally occurs in a hierarchical system of associations and clusters (e.g. Elmegreen 1997), the period of time over which a system will retain a non-diffuse morphology depends upon the mass and size distribution of the clusters. An unbound cluster of mass  $M$ , radius  $R$ , and velocity dispersion  $V \geq \sqrt{2GM/R}$  km s<sup>-1</sup> will disperse in a time of  $t < R/V$  years. For example, an unbound cluster of mass  $10^7 M_\odot$  and radius 100 pc will dissolve by an age of  $\sim 3$  Myr. The ten near-infrared-bright knots in NGC 7771 appear to be gravitationally bound since they remain distinct sources at an age of  $\approx 10$  Myr. The  $K$  band morphology of NGC 7469 may have a smoother appearance because some of the clusters in its ring may be diffusing, due to either the age of the system, differences in the mass or spatial extent of some of the clusters, or differences in the gravitational potential.

The dispersion (or disruption) of the clusters may be related to the existence of the AGN in one of the following manners. First, the presence of a diffuse component may indicate that the potential associated with a secondary stellar bar is disrupting some of the clusters and funneling material into the central regions of the galaxy. This may happen only at certain times in the history of a galaxy; Friedli & Martinet (1997) indicate that the morphology of a ring in a system with nested bars may be related to the relative phase of the bars and that the secondary bar is a transient feature. The link may also be more indirect, with the dispersion of clusters simply indicating that the system is old enough to have established a mechanism to fuel a central AGN. Friedli & Martinet (1997) also note that gas will not reach the nuclei of ringed systems characterized by very high star formation efficiencies. We postulate that some galaxies may only form very massive, compact, gravitationally bound clusters. These systems may not be able to host an AGN because the material which would fuel an AGN is locked up in the circumnuclear star forming regions. Consequently, the facts that NGC 7771 possesses a clumpier ring than NGC 7469 and does not contain an AGN may indicate that NGC 7771 is not old enough to have formed an AGN or that NGC 7771 may not be able to fuel an AGN. This interpretation is complicated by the possibility that the star formation in nuclear rings may be episodic. In this case, the morphology of the star formation may not be related to the age of the system or its ability to host an AGN. A study of a larger sample of ringed galaxies which do and do not possess AGN is needed to better address this issue.

## 8. Summary and Conclusions

The galaxy NGC 7771 is one of the 20 most radio-luminous galaxies in the northern hemisphere whose emission is dominated by star formation processes. Only two of these galaxies, NGC 7771 and NGC 7469, contain nuclear rings. These galaxies are also characterized by high infrared luminosities ( $L_{fir} \sim 10^{11} L_\odot$ ). The two ringed galaxies NGC 7771 and NGC 7469 thus provide a link between radio-luminous and infrared-luminous systems and classical, less-luminous

ringed systems.

The starburst ring in NGC 7771 was first identified at radio wavelengths (Neff & Hutchings 1992). In this paper, we provide a “high” resolution near-infrared image of this ring. The radio, near-infrared, and optical properties of the central 2 kpc are used to constrain the age and the stellar content of the starburst ring. The origin of the ring and the relationship between rings and AGN are also discussed. We find the following:

1. The diameter of the starburst ring is  $\approx 6''$  or 1.6 kpc, and is similar to that of “classical” nuclear rings. Since NGC 7771 is a barred galaxy, the ring could be associated with one or two Inner Lindblad Resonances (ILRs). An  $H\alpha$  rotation curve identifies one possible ILR. This ILR is located exterior to the starburst ring, however. Additional kinematic data, obtained at longer wavelengths where optical depth effects are less severe, are needed to properly confirm or rule out a resonance origin for this ring.

2. The circumnuclear ring in NGC 7771 is heavily obscured, as evidenced by the *JHK* morphology and the  $H\alpha/H\beta$  line ratio. The dust obscuring the ionized gas by  $A_V \approx 6.5$  mag lies largely in front of the ionized gas. The near-infrared continuum emission may be less heavily obscured (e.g.  $A_V \sim 3$  mag). Alternatively, the geometry of the dust obscuring the continuum sources may differ from that obscuring the ionizing gas.

3. The starburst ring contains  $\approx 10$  near-infrared bright clumps and  $\approx 10$  radio-bright clumps  $\lesssim 300$  pc in diameter. Data with higher spatial resolution are needed to further constrain the physical sizes of the clumps. The number of clumps agrees with that predicted by the Elmegreen (1994) models of starburst rings associated with ILRs.

4. The near-infrared and radio sources are not spatially coincident. As in the southern ringed galaxy ESO 565 – 11 (Buta, Purcell, & Crocker 1995), this displacement is interpreted in terms of multiple generations of star formation. The displacement may reflect the rotation of the ring and/or propagating star formation.

5. Depending upon the exact value of the spectral index of the radio emission, the average thermal emission associated with each radio-bright knot is estimated to be equivalent to that of 35000 O6 stars. The average amount of non-thermal emission per knot is 35 times that of the most luminous radio source in M82. The corresponding supernovae rate is  $0.010 \text{ yr}^{-1}$  per knot. Deep 2 cm and 6 cm maps with comparable high spatial resolution would place stronger constraints upon the properties of the radio emitting knots.

6. The near-infrared emission is dominated by red supergiants. The average near-infrared knot flux is equivalent to that of  $\sim 5000$  red supergiants. Each near-infrared bright knot could contain 15 M 82-type clusters, as measured by Satyapal et al. (1997). These estimates could be improved by obtaining high spatial resolution *K* band spectra.

7. The radio knots and the near-infrared knots are estimated to be  $\approx 4$  to 8 Myr old and  $\approx 10$  Myr old, respectively. High resolution imagery in the  $\text{Br}\gamma$  recombination line and in the 2.3



$\mu\text{m}$  CO bandhead region would confirm the relative ages of the radio and near-infrared bright knots. In the current analysis, stellar population models predict that each knot has a total stellar mass of  $\sim 10^7 M_\odot$ . Similar cluster masses are observed in other starburst systems.

8. The time-averaged star formation rate is  $\sim 40 M_\odot \text{ yr}^{-1}$ . A comparison with the far-infrared luminosity reveals that the data are consistent with models which predict that a ring associated with an ILR will produce at least 50% of the total star formation.

9. While NGC 7771 contains a very clumpy ring and shows no evidence of AGN activity, NGC 7469 exhibits more diffuse emission and contains a Seyfert 1 nucleus. We suggest that the differences in morphology are related to the mechanism responsible for fueling the AGN. If the starburst in NGC 7771 is younger than that occurring in NGC 7469, the mechanism responsible for fueling an AGN may not have turned on yet in NGC 7771. Alternatively, the properties of the starburst in NGC 7771 may be such that gas cannot reach the nucleus to fuel an AGN. This interpretation is complicated by the possibility that star formation in ringed systems may be episodic. In this case, the morphology of the star formation may be unrelated to a galaxy's ability to host an AGN. We plan to conduct a systematic study of a larger sample of ringed systems in order to better understand this issue.

We wish to thank Ron Buta for thoughtful and timely comments which improved both the content and the presentation of this paper. We also thank Ron Allen, Ralph Bohlin, Anne Kinney, and Claus Leitherer for helpful discussions, and Bill Keel for providing an electronic version of the H $\alpha$  rotation curve. Portions of this work were completed while DAS was supported by a National Research Council-GSFC Research Associateship. This research is also supported by NSF grants AST-9528860 to MPH and TH and AST-9023450 to MPH. The authors have made use of the NASA/IPAC Extragalactic Database (NED) which is operated by the Jet Propulsion Laboratory, Caltech, under contract with the National Aeronautics and Space Administration.

## REFERENCES

- Batuski, D. J., Hanisch, R. J., & Burns, J. O., 1992, *AJ*, 103, 1077
- Benedict, G. F., Smith, B. J., & Kenney, J. D. P. 1996, *AJ*, 111, 1861
- Binney, J., & Tremaine, S. 1987, *Galactic Dynamics* (Princeton: Princeton University Press)
- Bosma, A., Byun, Y., Freeman, K. C., & Athanassoula, E. 1992, *ApJ*, 400, L21
- Bruzual, G. A., & Charlot, S. 1993, *ApJ*, 405, 538
- Burns, J. O., Hanisch, R. J., White, R. A., Nelson, E. R., Morrisette, K. A., & Moody, J. W., 1987, *AJ*, 94, 587
- Buta, R. 1986a, *ApJS*, 61, 609
- Buta, R. 1986b, *ApJS*, 61, 631
- Buta, R. 1988, *ApJS*, 66, 233
- Buta, R. 1990, *ApJ*, 351, 62
- Buta, R., & Crocker, D. A. 1993, *AJ*, 105, 1344
- Buta, R., Purcell, G. B., & Crocker, D. A. 1995, *AJ*, 110, 1588
- Buta, R., & Purcell, G. B. 1998, *ApJ*, 115, 484
- Calzetti, D., Kinney, A. L., & Storchi–Bergmann, T. 1994, *ApJ*, 429, 582
- Calzetti, D., 1997, *AJ*, 113, 162
- Carico, D. P., Sanders, D. B., Soifer, B. T., Elias, J. H., Matthews, K., and Neugebauer, G. 1988, *AJ*, 95, 356
- Cerviño, M., & Mas–Hesse, J. M. 1994, *A&A*, 284, 749 (CMH94)
- Condon, J. J. & Yin, Q. F. 1990, *ApJ*, 357, 97
- Condon, J. J., Frayer, D. T., & Broderick, 1991, *AJ*, 101, 362
- Condon, J. J. 1992, *ARA&A*, 30, 575
- Devereux, N. A., Becklin, E. E., & Scoville, N. 1987, *ApJ*, 312, 529
- Devereux, N. A. 1989, *ApJ*, 346, 126
- Devereux, N. A., Kenney, J. D. P., & Young, J. S. 1992, *AJ*, 103, 784
- Downes, D., & Solomon, P. M., 1998, *ApJ*, in press
- Doyon, R., Joseph, R. D., & Wright, G. S. 1994, *ApJ*, 421, 101
- Duric, N., & Dittmar, M. R. 1988, *ApJ*, 332, L67
- Eales, S. A., Becklin, E. E., Hodapp, K. -W., Simons, D. A., & Wynn–Williams, C. G., 1990, *ApJ*, 365, 478
- Elmegreen, B. G. 1994, *ApJ*, 425, L73

- Elmegreen, B. G. 1997, *RevMexAA (Serie de Conferencias)*, 6, 165
- Friedli, D., & Martinet, L. 1997, *RevMexAA (Serie de Conferencias)*, 6, 177
- Frogel, J. A., Persson, S. E., Aaronson, M., & Matthews, K. 1978, *ApJ*, 220, 75
- Garcia, A. M. 1993, *A&AS*, 100, 47
- Genzel, R., Weitzel, L., Tacconi–Garman, L. E., Blietz, M., Cameron, M., Krabbe, A., Lutz, D., & Sternberg, A. 1995, *ApJ*, 444, 129
- Golla, G., Allen, M. L., & Kronberg, P. P. 1996, *ApJ*, 473, 244
- Gordon, K. D., Calzetti, D., & Witt, A. N. 1997, *ApJ*, 487, 625 (GCW)
- Goldader, J. D., Joseph, R. D., Doyon, R., & Sanders, D. B. 1997, *ApJ*, 474, 104
- Ho, L. C., Filippenko, A. V., & Sargent, W. L. W. 1997, *ApJ*, 487, 591
- Hutchings, J. B., 1989, *AJ*, 98, 524
- Joseph, R. D., Meikle, W. P. S., Robertson, N. A., & Wright, G. S. 1984, *MNRAS*, 209, 111
- Kalas, P., & Wynn–Williams, C. G. 1994, *ApJ*, 434, 546
- Karachentsev, I. D. 1987, *Dvoinye Galaktiki (Nauka, Moscow)*
- Keel, W. C. 1993, *AJ*, 106, 1771
- Keel, W. C. 1996, *ApJS*, 106, 27
- Koornneef, J. 1983, *A&A*, 128, 84
- Kronberg, P. P., Biermann, P., & Schwab, F. R. 1985, *ApJ*, 291, 693
- Lançon, A., & Rocca–Volmerange, B. 1996, *New Astronomy*, 1, 215
- Larkin, J. E., Graham, J. R., Matthews, K., Soifer, B. T., Beckwith, S., Herbst, T. M., & Quillen, A. C. 1994, *ApJ*, 420, 159
- Leitherer, C., & Heckman, T. M. 1995, *ApJS*, 96, 9
- Lester, D. F., Carr, J. S., Joy, M., & Gaffney, N. 1990, *ApJ*, 352, 544
- Maiolino, R., Ruiz, M., Rieke, G. H., & Papadopoulos, P. 1997, *ApJ*, 485, 552
- Maoz, D., Barth, A. J., Sternberg, A., Filippenko, A. V., Ho, L. C., Macchetto, F. D., Rix, H. W., & Schneider, D. P. 1996, *AJ*, 111, 2248
- Mas–Hesse, J. M., & Kunth, D. 1991, *A&AS*, 88, 399 (MHK91)
- McLeod, K. K., Rieke, G. H., Rieke, M. J., & Kelly, D. M. 1993, *ApJ*, 412, 111
- Meurer, G. R., Heckman, T. M., Leitherer, C., Kinney, A., Robert, C., & Garnett, D. R. 1995, *AJ*, 110, 2665
- Miller, G. E., & Scalo, J. M. 1979, *ApJS*, 41, 513
- Neff, S. G., & Hutchings, J. B., 1992, *AJ*, 103, 1746

- Nordgren, T. E., Chengalur, J. N., Salpeter, E. E., & Terzian, Y. 1997, *AJ*, 114, 77
- Osman, A. M. I. 1986, *Ap&SS*, 124, 345
- Panagia, N. 1973, *AJ*, 78, 929
- Pfenniger, D. & Norman, C. 1990, *ApJ*, 363, 391
- Rieke, G. H., Loken, K., Rieke, M. J., & Tamblyn, P. 1993, *ApJ*, 412, 99
- Sams, B. J., III, Genzel, R., Eckart, A., Tacconi–Garman, L., & Hofmann, R. 1994, *ApJ*, 430, L33
- Sanders, D. B., Scoville, N. Z., Young, J. S., Schloerb, F. P., Rice, W. L., & Danielson, G. E., 1986, *ApJ*, 305, L45
- Satyapal, S., Watson, D. M., Pipher, J. L., Forrest, W. J., Coppenger, D., Raines, S. N., Libonate, S., Riché, F., Greenhouse, M. A., Smith, H. A., Thompson, K. L., Fisher, J., Woodward, C. E., & Hodge, T. 1995, *ApJ*, 448, 611
- Satyapal, S., Watson, D. M., Pipher, J. L., Forrest, W. J., Greenhouse, M. A., Smith, H. A., Fischer, J., & Woodward, C. E. 1997, *ApJ*, 483, 148
- Schmidt–Kaler, Th. 1982, in Landolt–Börnstein, Vol. VI/2b, Stars and Star Clusters, ed. K. Schaifers and H. H. Voigt (Berlin: Springer–Verlag), 451
- Schinnerer, E., Eckart, A., Quirrenbach, A., Böker, T., Tacconi–Garman, L. E., Krabbe, A., & Sternberg, A. 1997, *ApJ*, 488, 174
- Shlosman, I., Frank, J., & Begelman, M. C. 1989, *Nature*, 338, 45
- Shlosman, I., Begelman, M. C., & Frank, J. 1990, *Nature*, 345, 679
- Simkin, S. M., Su, H. J., & Schwarz, M. P. 1980, *ApJ*, 237, 404
- Smith, D. A., Herter, T., Haynes, M. P., Beichman, C. A., & Gautier, T. N. 1995, *ApJ*, 439, 623
- Smith, D. A., Herter, T., Haynes, M. P., Beichman, C. A., & Gautier, T. N. 1996, *ApJS*, 104, 217
- Smith, D. A., et al. 1996b, *ApJ*, 473, L21
- Smith, D. A., Herter, T., Haynes, M. P. 1998, *ApJ*, 494, 150
- Telesco, C. M., Dressel, L. L., & Wolstencroft, R. D. 1993, *ApJ*, 414, 120
- Storchi–Bergmann, T., Wilson, A. S., & Baldwin, J. A. 1996, *ApJ*, 460, 252
- Telesco, C. M., & Decher, R. 1988, *ApJ*, 334, 573
- Telesco, C. M. 1988, *ARA&A*, 26, 343
- Telesco, C. M., Campins, H., Joy, M., Dietz, K., & Decher, R. 1991a, *ApJ*, 369, 135
- Telesco, C. M., Joy, M., Dietz, K., Decher, R., & Campins, H. 1991b, *ApJ*, 369, 135
- Thronson, H. A., Jr., & Greenhouse, M. A. 1988, *ApJ*, 327, 671
- Turner, P. C., Forrest, W. J., Pipher, J. L., & Shure, M. A. 1992, *ApJ*, 393, 648
- Ulvestad, J. S., & Antonucci, R. R. J. 1997, *ApJ*, 488, 621

- Veilleux, S., Kim, D. -C., Sanders, D. B., Mazzarella, J. M., & Soifer, B. T. 1995, *ApJS*, 98, 171
- Whittet, D. C. B. 1992, *Dust in the Galactic Environment* (Bristol: IOP)
- Wilson, A. S., Helfer, T. T., Haniff, C. A., & Ward, M. J. 1991, *ApJ*, 381, 79

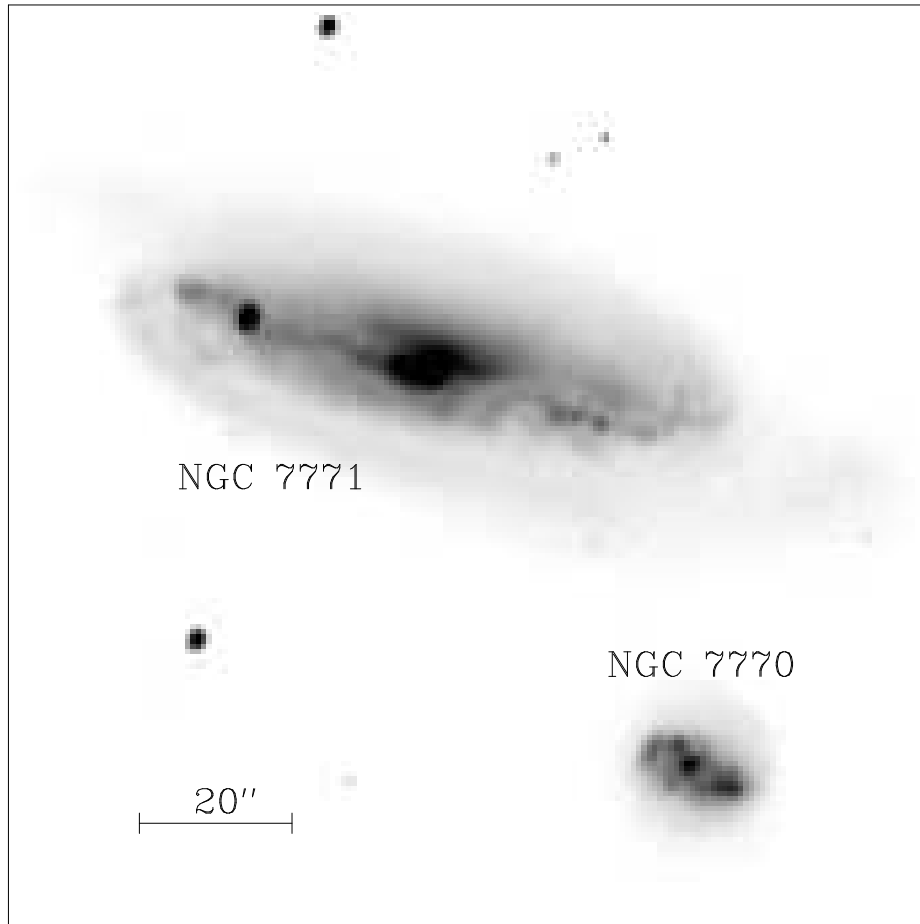


Fig. 1.— Global Morphology. This *I* band image obtained by R. Giovanelli and M. Haynes (see text) shows the global morphology of NGC 7771 and its nearest companion in projection, NGC 7770. The optical morphology of NGC 7771 is strongly affected by extinction and interactions. The scale bar represents  $20''$ , or 5.5 kpc.

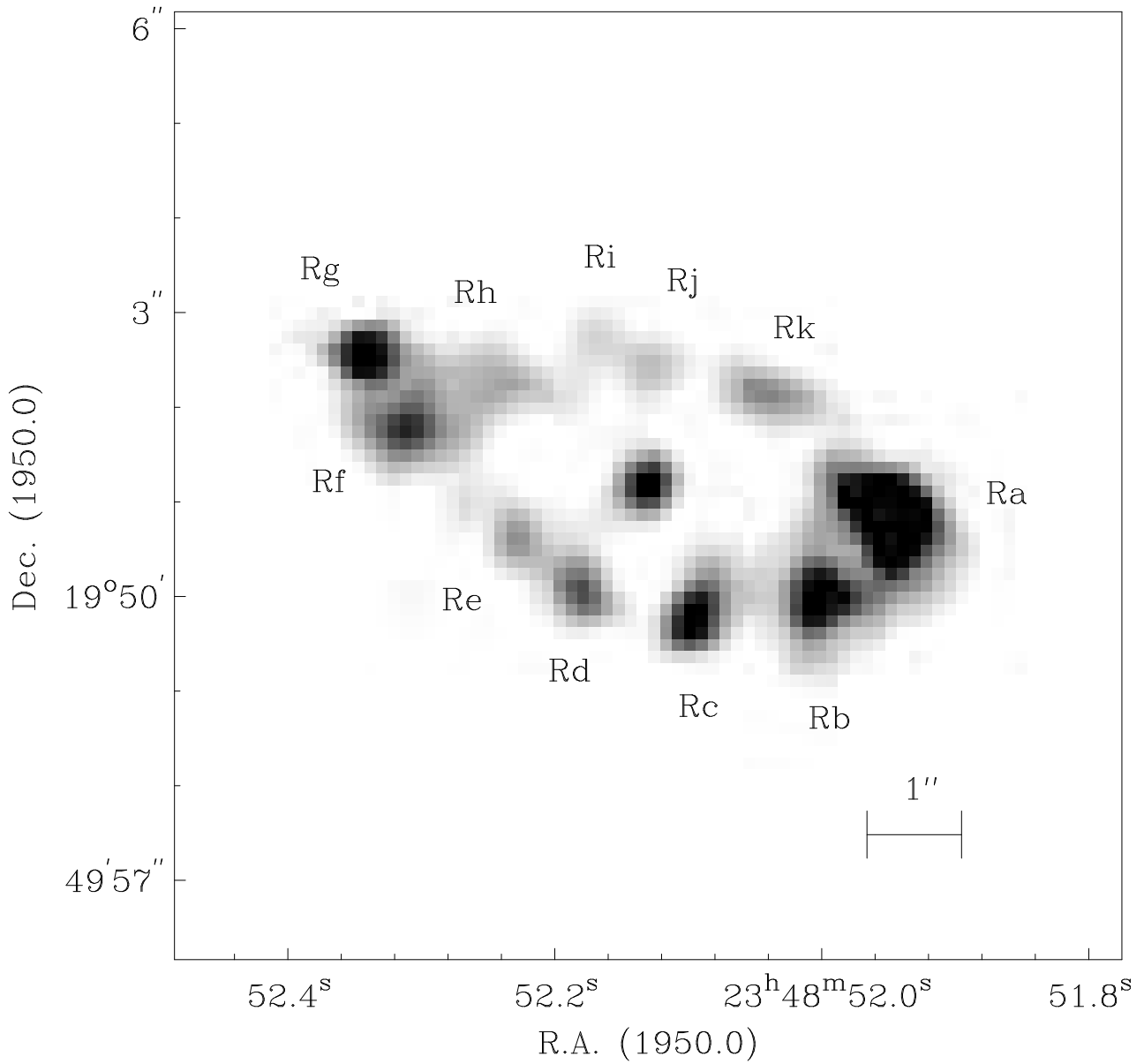


Fig. 2.— Radio Data from Neff & Hutchings (1992). The 6 cm emission from the central 14'' of NGC 7771 is shown above. North is up, and east is to the left. The radio data have been tapered and restored with a  $0.55'' \times 0.52''$  FWHM Gaussian beam. Eleven knots, denoted Ra–Rk, form a circumnuclear ring of emission. The scale bar represents 1'', or 275 pc.

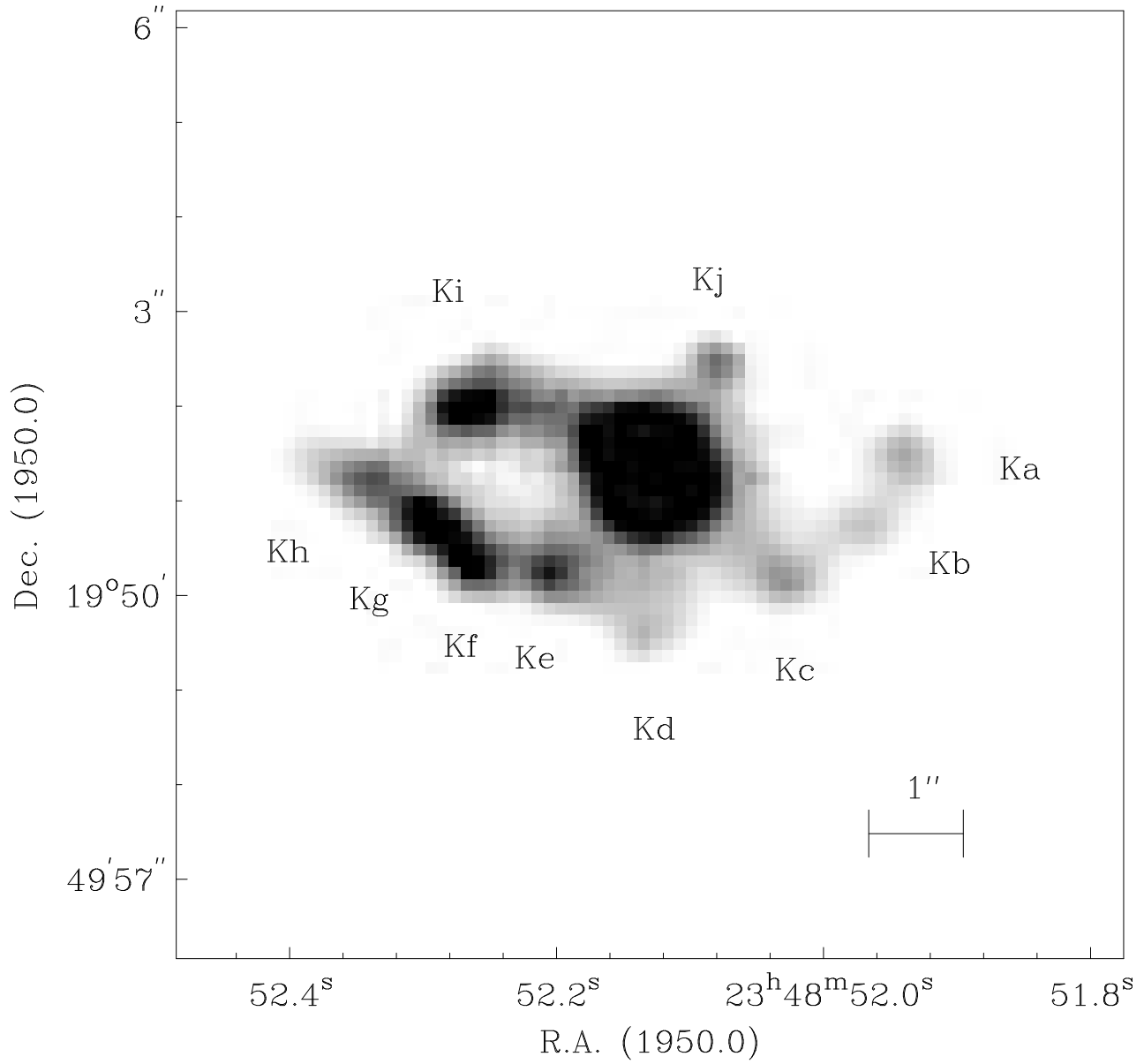


Fig. 3.— K band image. The distribution of the K band emission is illustrated above. The field of view, orientation, and scale are as in Figure 2. Ten knots, denoted Ka–Kj, form a circumnuclear ring.



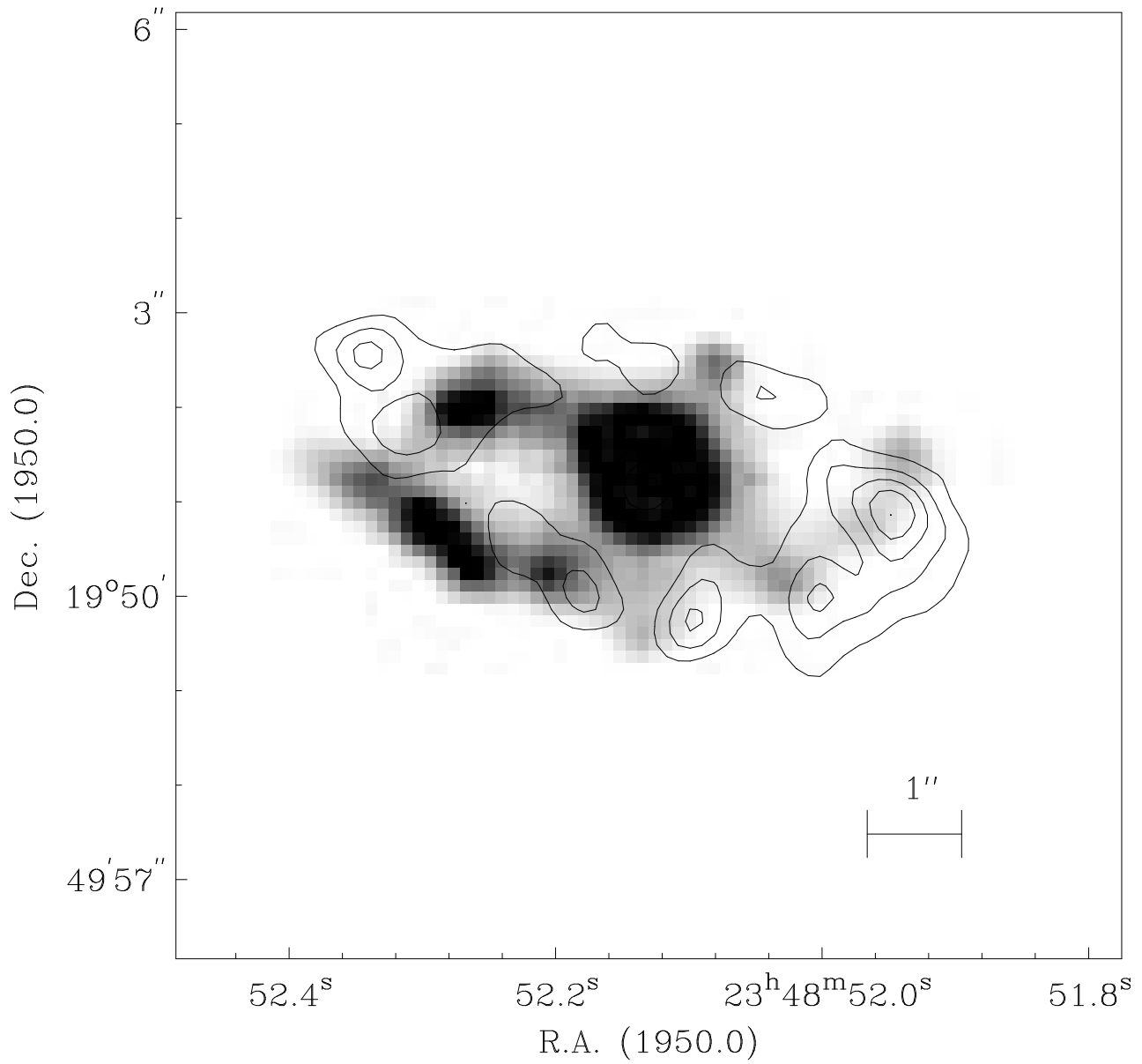


Fig. 4.— K band and 6 cm emission. The K band emission is shown in greyscale along with contours representing the 6 cm emission. The field of view, orientation, and scale are as in Figure 2. The peaks of the near-infrared and the radio emission are not spatially coincident.

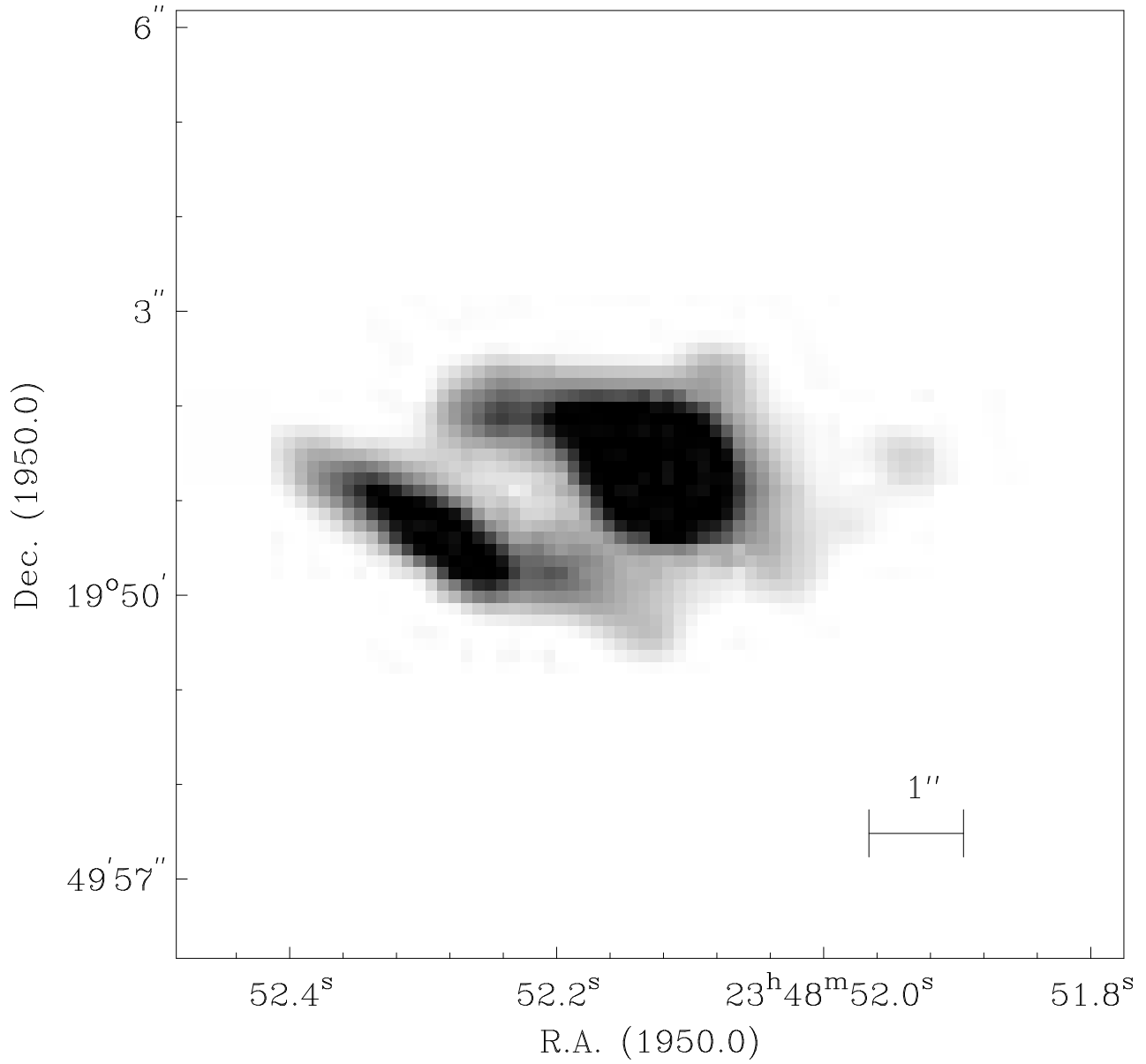


Fig. 5.— H band image. Same as Figure 3, for the H band. The H band emission is smoother than the K band emission.

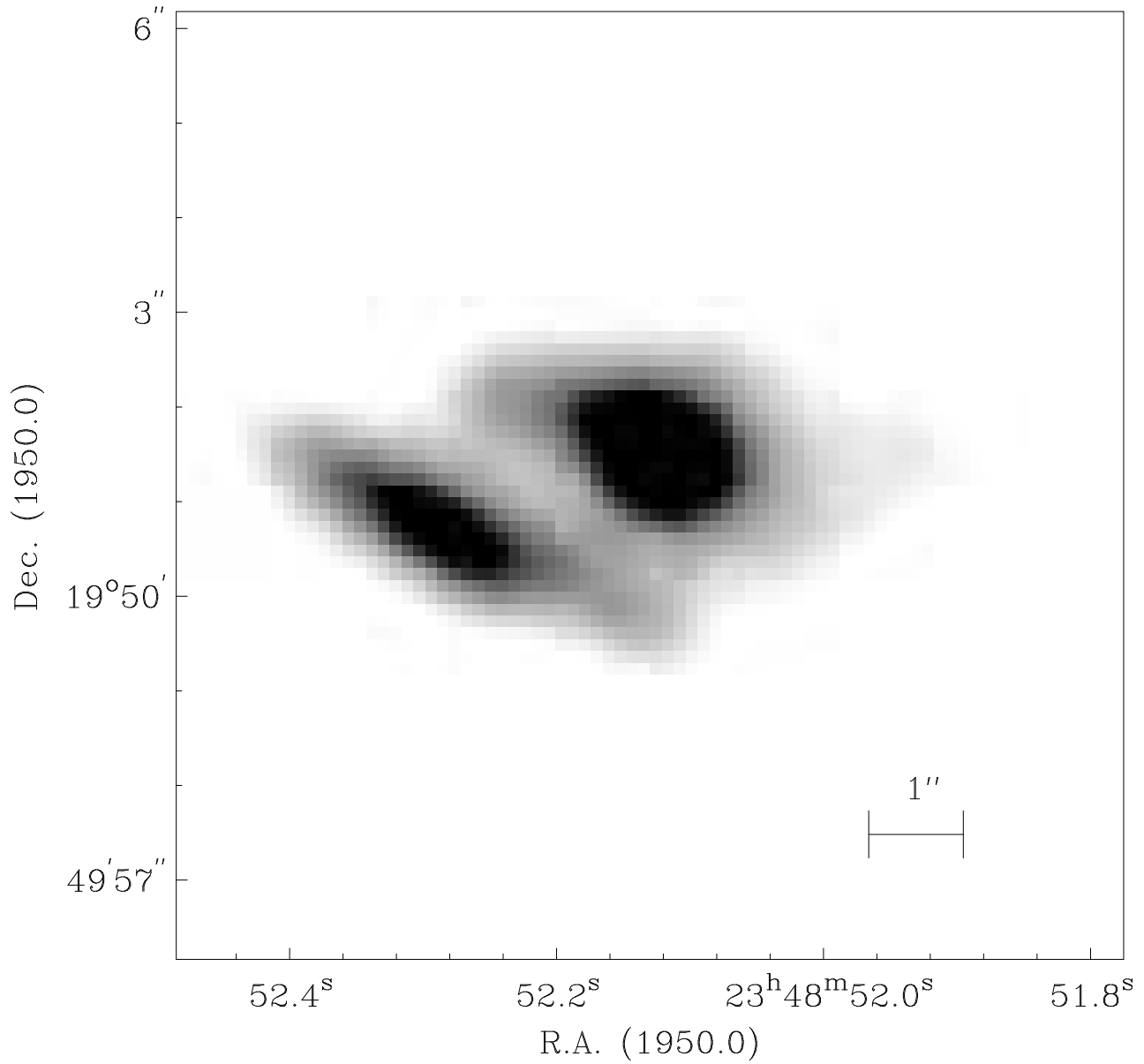


Fig. 6.— J band image. Same as Figure 3, for the J band. With the exception of knot Kg, the clumps comprising the circumnuclear ring are fading into the diffuse background emission from NGC 7771.

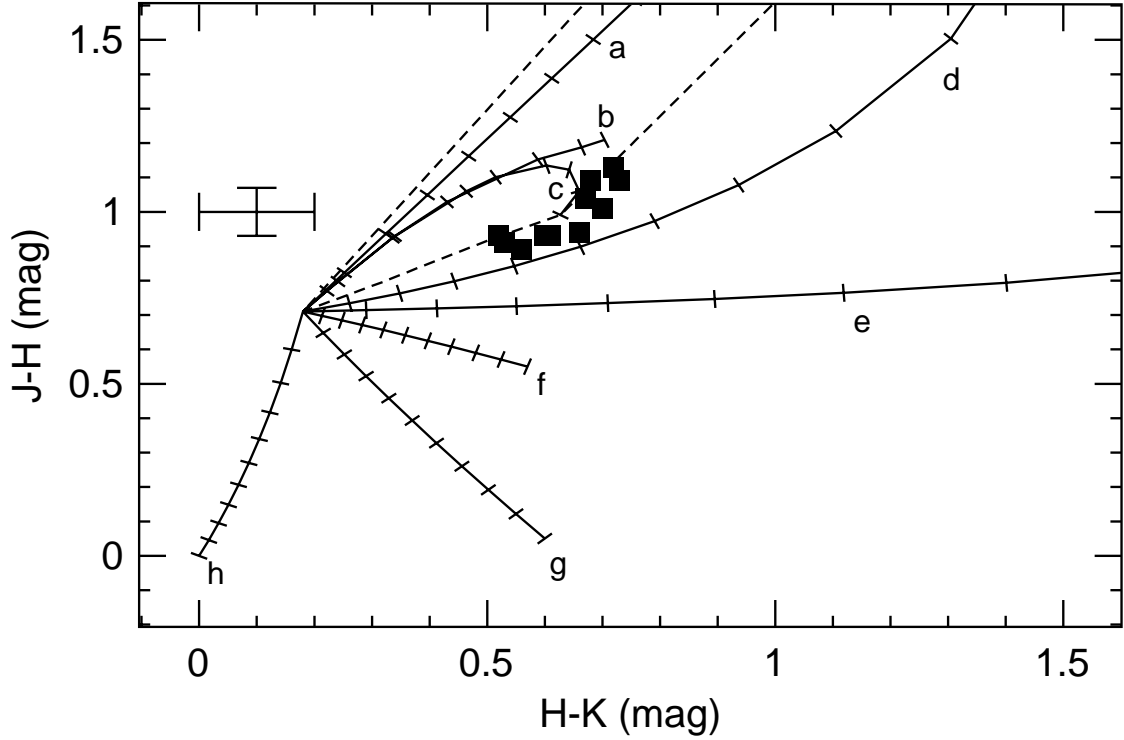


Fig. 7.— Near-Infrared Knot Colors. The colors of knots Ka–Kj and the nucleus are shown above. Curves illustrate the effects of a) an external dust screen, b) dust mixed uniformly with stars, c) an obscuring shell of dust, d) dust emission at 1000K with  $\epsilon \propto 1/\lambda$ , e) dust emission at 500K with  $\epsilon \propto 1/\lambda$ , f) synchrotron emission, g) thermal gas emission from HII regions and h) blue stars, on the intrinsic colors of red giants and supergiants ( $H - K = 0.18$  mag;  $J - H = 0.71$  mag). For curves d) through h), tick marks indicate the percentage contribution of each mechanism at  $K$ , in increments of 10%. For curve a), the interval between tick marks is 1 mag. For curve b), tick marks are shown for  $A_V = 1.5, 6, 10, 20, 30$ , and 40 mag. For curve c), tick marks are shown for  $A_V = 1.5, 4, 8, 10, 15, 20, 30$ , and 40 mag. The dotted line outlines the region covered by additional reddening models available in the literature. All measurements and models have been converted to the CIT photometric system.

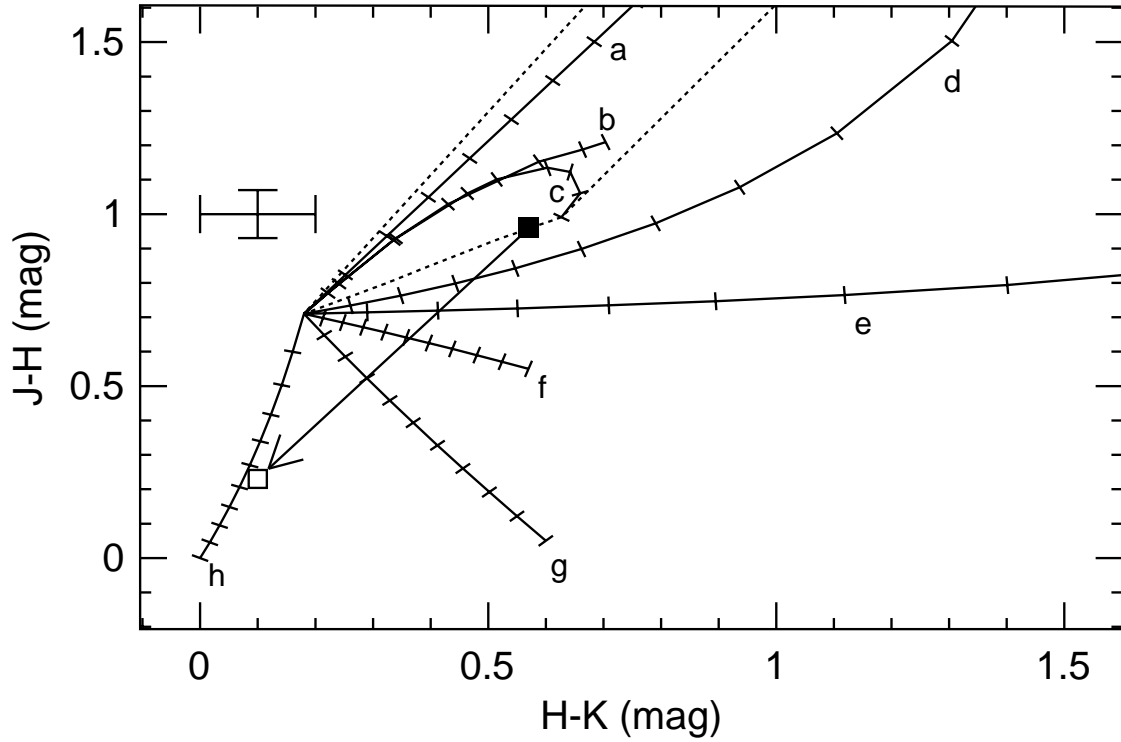


Fig. 8.— Near-Infrared Emission Processes. The solid square represents the colors of the region for which the  $H\alpha/H\beta$  line ratio has been measured. The arrow pointing to the open square shows how the colors change after a correction for  $A_V = 6.5$  magnitudes of extinction. Curves a) through h) are the same as in Figure 7.

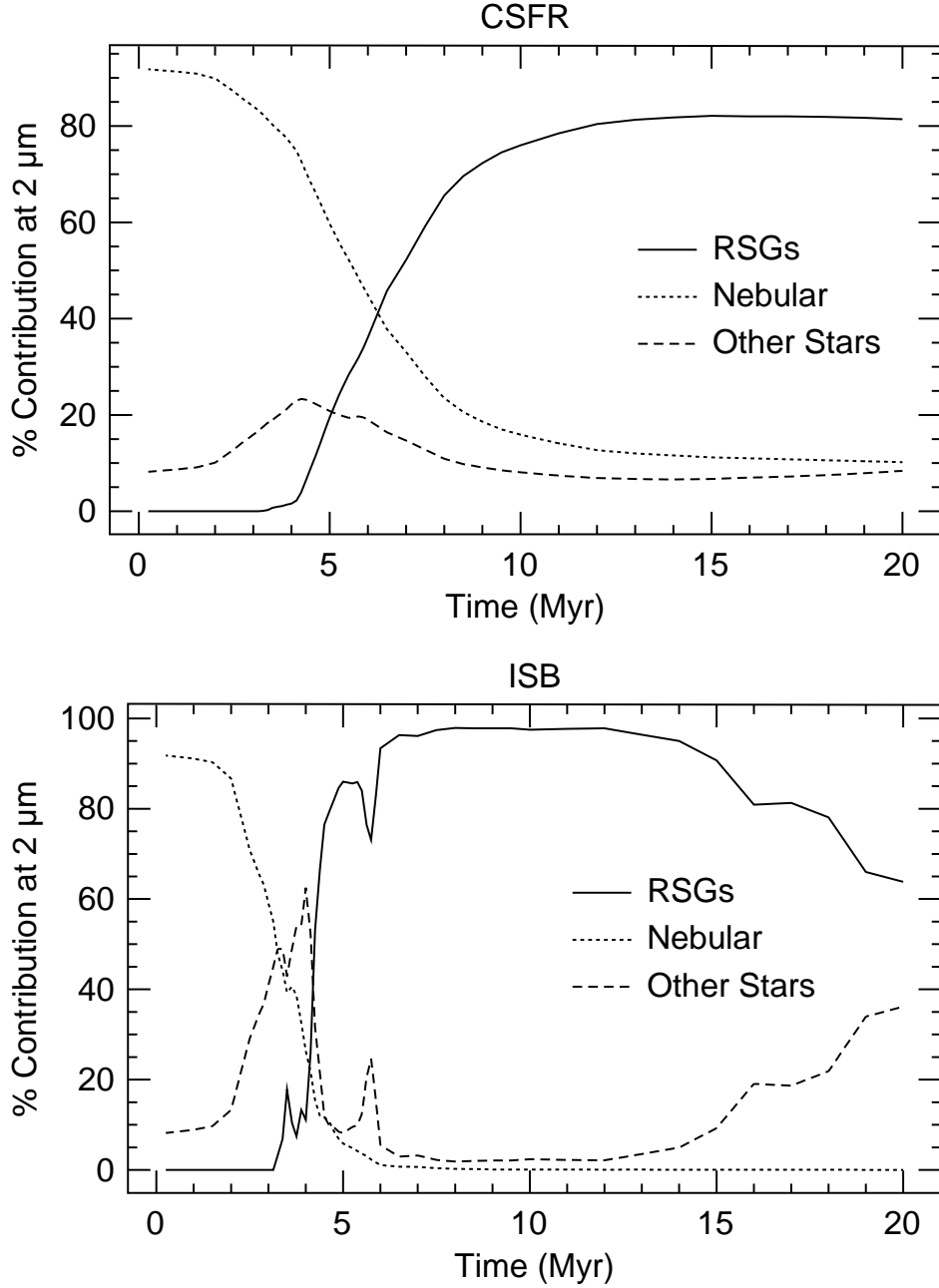


Fig. 9.— The Role of Red Supergiants (RSGs). The percentage of the  $2 \mu\text{m}$  luminosity produced by red supergiants, nebular emission, and other stars is shown for a constant star formation rate (CSFR) and an instantaneous burst (ISB). The data are taken from CMH94.

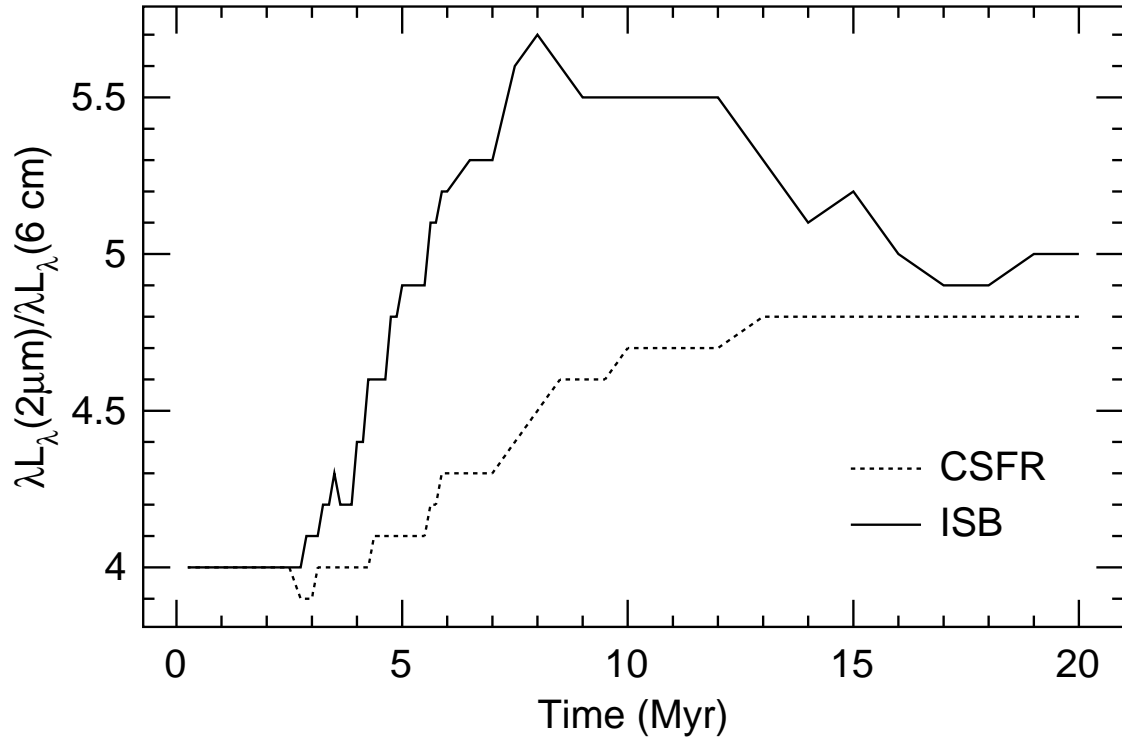


Fig. 10.— The Ratio of the Near-Infrared and Radio Luminosities. The ratio of the 2  $\mu\text{m}$  and the 6 cm luminosities is illustrated as a function of time for a constant star formation rate (CSFR) and an instantaneous burst (ISB), as calculated by CMH94.

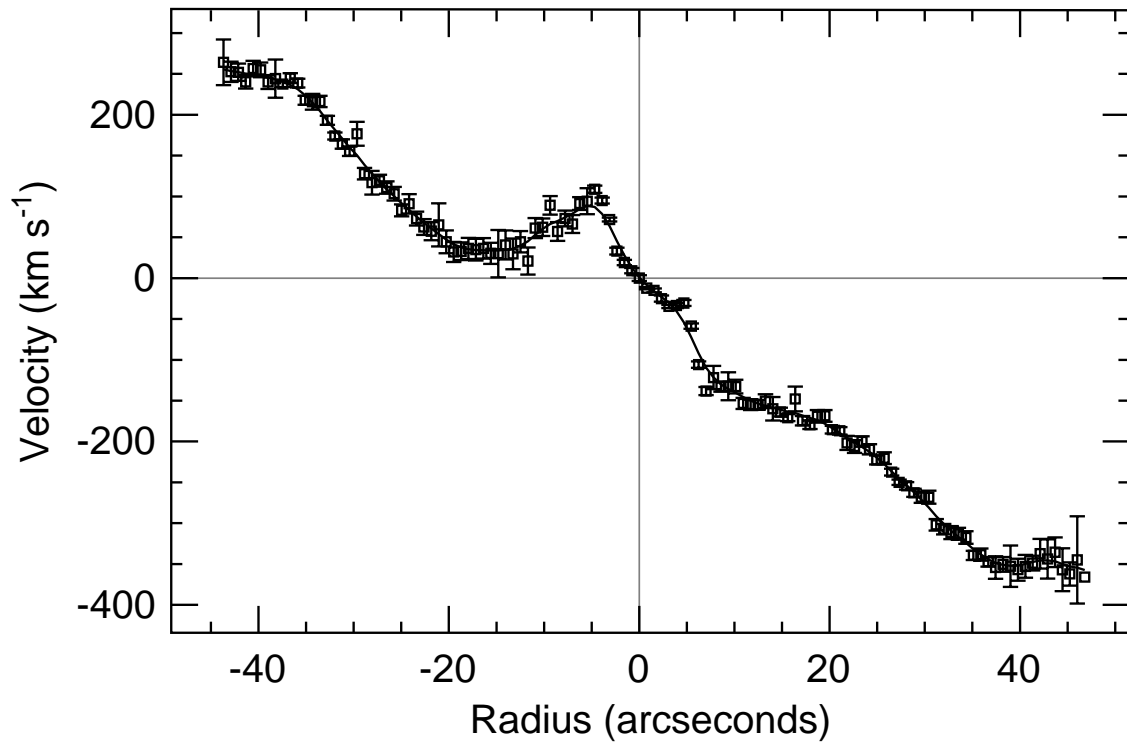


Fig. 11.— H $\alpha$  Rotation Curve. The H $\alpha$  rotation curve obtained by Keel (1996) is displayed above, corrected for inclination. The error bars represent a two sigma level uncertainty in the velocity.



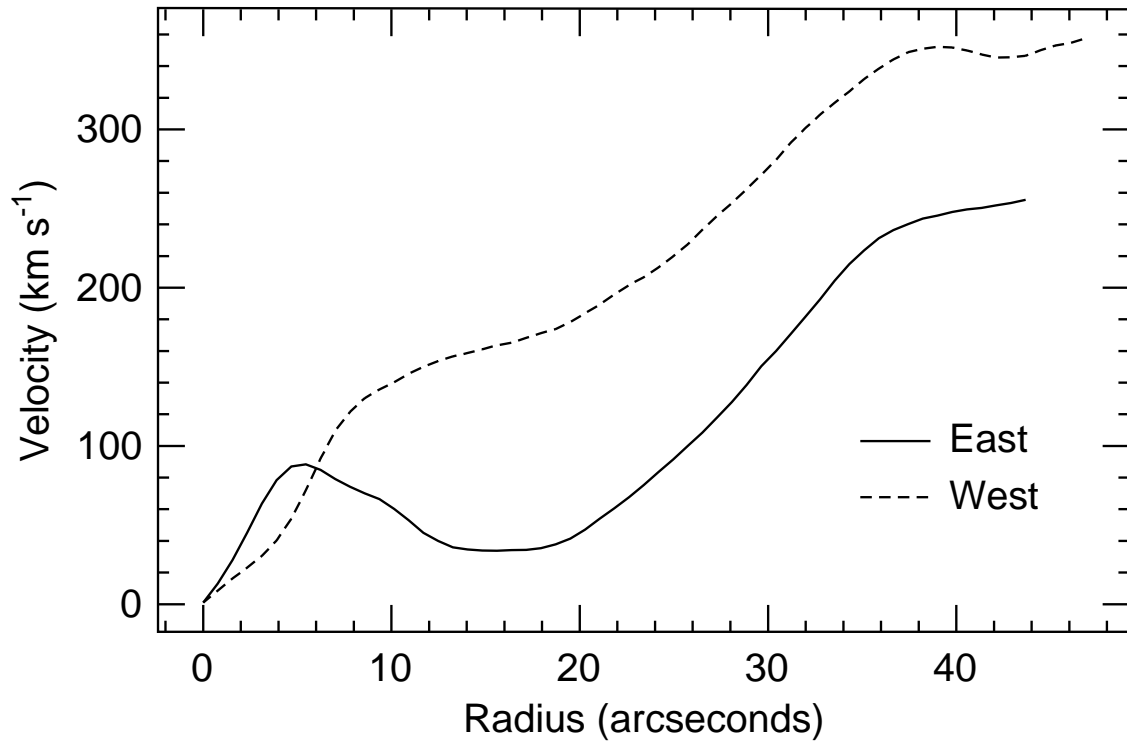


Fig. 12.— Folded H $\alpha$  rotation curve. The smoothed H $\alpha$  rotation curve is shown folded about the peak of the continuum emission. Note the discrepancy between the eastern and western sides of the curve.

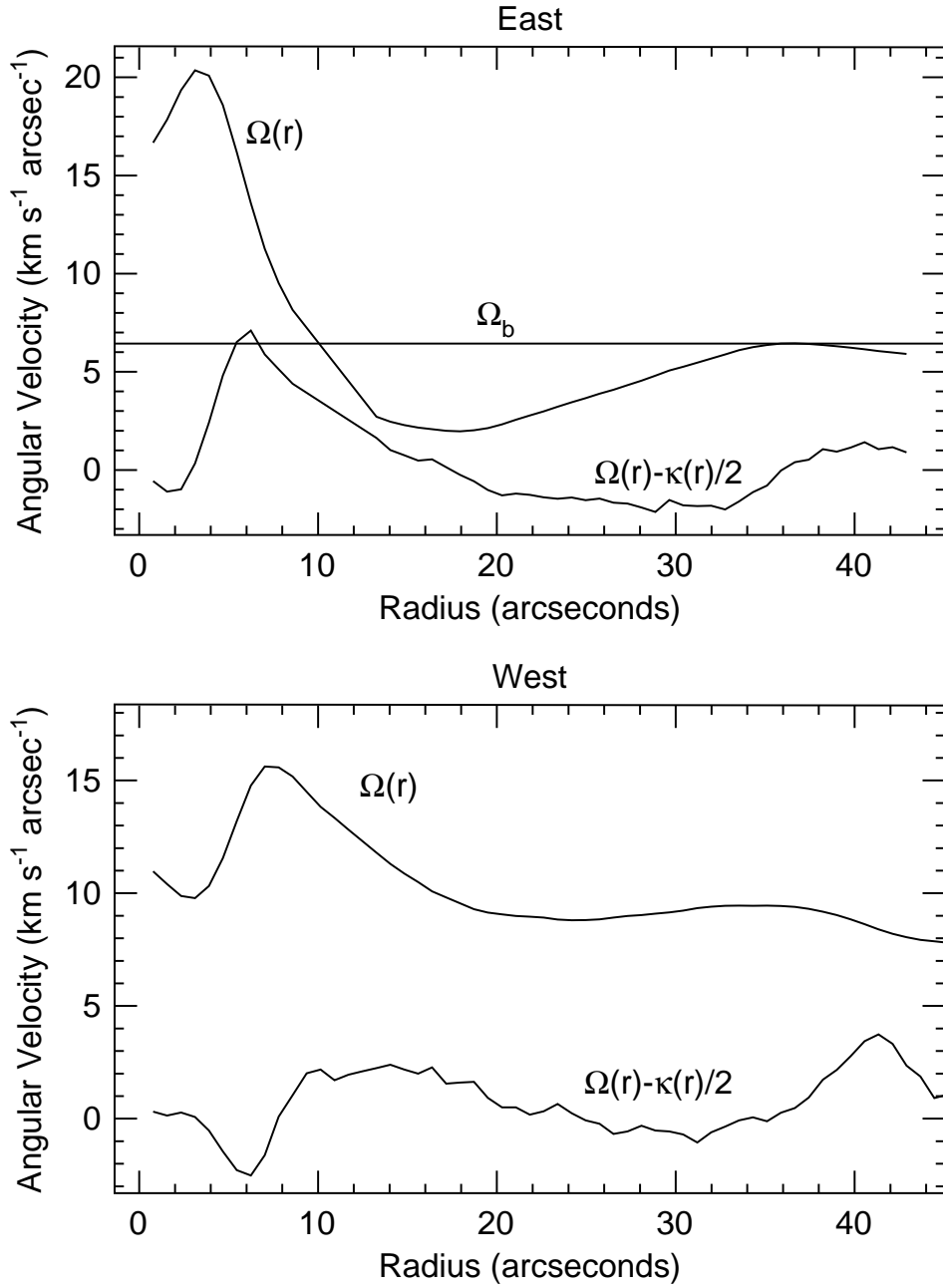


Fig. 13.— Resonances. The angular velocities ( $\Omega(r)$ ) derived from the eastern and western portions of the smoothed H $\alpha$  rotation curve are illustrated above. The value of  $\Omega(r) - \kappa(r)/2$  is also given. For a bar pattern speed of  $\Omega_b = 6.4 \text{ km}^{-1} \text{ s}^{-1} \text{ arcsec}^{-1}$ , an ILR appears to be located at a radius of  $r \approx 6''$ . The western portion of the rotation curve does not show evidence of an ILR.

Table 1. Redshift–Corrected Near–Infrared Fluxes and Colors in a 0.75'' Diameter Aperture

Knot	$K$ (mJy)	$H$ (mJy)	$J$ (mJy)	$\sigma_K$ (mJy)	$\sigma_H$ (mJy)	$\sigma_J$ (mJy)	$H - K$ (mag)	$J - H$ (mag)	$\sigma_{H-K}$ (mag)	$\sigma_{J-H}$ (mag)
Ka	0.75	0.65	0.38	0.06	0.03	0.02	0.67	1.04	0.10	0.07
Kb	0.72	0.61	0.37	0.06	0.03	0.02	0.70	1.01	0.10	0.07
Kc	0.79	0.68	0.38	0.07	0.03	0.02	0.68	1.09	0.10	0.07
Kd	0.74	0.69	0.45	0.06	0.03	0.02	0.60	0.93	0.11	0.07
Ke	0.90	0.83	0.54	0.08	0.03	0.03	0.61	0.93	0.10	0.07
Kf	0.93	0.93	0.60	0.08	0.04	0.03	0.52	0.93	0.11	0.07
Kg	0.97	0.96	0.63	0.08	0.04	0.03	0.53	0.91	0.11	0.07
Kh	0.87	0.84	0.56	0.08	0.04	0.03	0.56	0.89	0.11	0.07
Ki	0.96	0.79	0.44	0.08	0.03	0.02	0.73	1.09	0.10	0.07
Kj	0.78	0.69	0.44	0.07	0.03	0.02	0.66	0.94	0.10	0.07
N	1.54	1.29	0.69	0.13	0.05	0.03	0.72	1.13	0.10	0.07

Note. — All colors are redshift–corrected and are on the CIT photometric system. A 0.75'' diameter aperture extracts 50% of the total flux for a point source observed with 0.6'' seeing.

Table 2. 6 cm Fluxes of Radio-Bright Knots  
(0.75'' Diameter Aperture)

Knot	Flux (mJy)
Ra	2.12
Rb	1.54
Rc	1.42
Rd	1.20
Re	1.05
Rf	1.39
Rg	1.50
Rh	1.07
Ri	0.85
Rj	0.91
Rk	1.08
N	1.31

Table 3. Properties of the 6 cm Emission

Region	Total Flux (mJy)	Spectral Index	Thermal Flux (mJy)
Global	54 <sup>a</sup>	0.62 <sup>a</sup>	24.8
Ring	29.4 <sup>b</sup>	...	...
Nucleus	4.2 <sup>b</sup>	...	...
Ring + Nucleus	33.6 <sup>b</sup>	0.50 <sup>d</sup>	20.7
Ring + Nucleus	33.6 <sup>b</sup>	0.83 <sup>e</sup>	4.4
Disk	20.4 <sup>c</sup>	0.8	4.1
Disk	20.4 <sup>c</sup>	0.1	20.4

<sup>a</sup>From Condon et al. (1991) single dish measurements.

<sup>b</sup>From Neff & Hutchings (1992) VLA imaging data.

<sup>c</sup>Estimated from the difference between the single dish and VLA measurements.

<sup>d</sup>Estimated assuming the disk emission is non-thermal ( $\alpha = 0.8$ ).

<sup>e</sup>Estimated assuming the disk emission is thermal ( $\alpha = 0.1$ ).

Table 4. Stellar Content of Infrared–Bright Knots

Knot (1)	$M_K$ (2)	$N_{clus}$ (3)	$N_{RSG}$ (4)
Ka	-19.99	13	4800
Kb	-19.95	12	4600
Kc	-20.05	14	5000
Kd	-19.98	13	4700
Ke	-20.19	16	5700
Kf	-20.23	16	5900
Kg	-20.27	17	6200
Kh	-20.16	15	5500
Ki	-20.26	17	6100
Kj	-20.04	14	4900
N	-20.78	27	9800

Note. — (1) Knot name. (2) Absolute  $K$  band magnitude, including a factor of 2 aperture correction and an  $A_K = 0.3$  mag extinction correction. (3) Number of M 82–type clusters, derived from column 2. (4) Number of equivalent K4 supergiants, derived from column 2.

Table 5. Supernovae Content of Radio-Bright Knots

Knot (1)	$L_{NT}$ (2)	$\nu_{SN}$ (3)	$N_{M\ 82}$ (4)	$N_{41.9+58}$ (5)
Ra	$6.20 \times 10^{20}$	0.017	1450	58
Rb	$4.50 \times 10^{20}$	0.012	1050	42
Rc	$4.15 \times 10^{20}$	0.011	970	38
Rd	$3.51 \times 10^{20}$	0.0095	820	33
Re	$3.07 \times 10^{20}$	0.0084	720	28
Rf	$4.06 \times 10^{20}$	0.011	950	38
Rg	$4.39 \times 10^{20}$	0.012	1030	41
Rh	$3.13 \times 10^{20}$	0.0085	730	29
Ri	$2.48 \times 10^{20}$	0.0068	580	23
Rj	$2.66 \times 10^{20}$	0.0072	620	25
Rk	$3.16 \times 10^{20}$	0.0086	740	29
N	$3.83 \times 10^{20}$	0.010	900	36

Note. — (1) Knot name. (2) 6 cm non-thermal luminosity, including a factor of 2 aperture correction ( $\text{W Hz}^{-1}$ ). (3) Supernovae rate ( $\text{yr}^{-1}$ ). (4) Number of M 82-type supernovae. (5) Number of 41.9 + 58 type supernovae.

Table 6. Ionization Properties of Radio-Bright Knots

Knot (1)	$N_{UV}$ (2)	$N_{O6V}$ (3)
Ra	$7.0 \times 10^{53}$	59000
Rb	$5.1 \times 10^{53}$	42000
Rc	$4.7 \times 10^{53}$	39000
Rd	$4.0 \times 10^{53}$	33000
Re	$3.5 \times 10^{53}$	29000
Rf	$4.6 \times 10^{53}$	38000
Rg	$5.0 \times 10^{53}$	41000
Rh	$3.6 \times 10^{53}$	30000
Ri	$2.8 \times 10^{53}$	24000
Rj	$3.0 \times 10^{53}$	25000
Rk	$3.6 \times 10^{53}$	30000
N	$4.3 \times 10^{53}$	36000

Note. — (1) Knot name. (2) Number of ionizing photons ( $s^{-1}$ ), including a factor of 2 aperture correction. (3) Number of equivalent O6V stars.